Quaternary International 503 (2019) 10–23

Contents lists available at ScienceDirect

Quaternary International

journal homepage: www.elsevier.com/locate/quaint

Linkage between C_4 vegetation expansion and dune stabilization in the deserts of NE China during the late Quaternary

Licheng Guo[a,b,c,*], Shangfa Xiong[a,b,c,**], Xinxin Dong[d], Zhongli Ding[a,b,c], Ping Yang[e], Hua Zhao[f], Jiabin Wu[a,b,c], Wei Ye[e], Guiyun Jin[g], Wenwan Wu[g], Lin Zheng[h]

[a] Key Laboratory of Cenozoic Geology and Environment, Institute of Geology and Geophysics, Chinese Academy of Sciences, Beijing, 100029, China
[b] University of Chinese Academy of Sciences, Beijing, 100049, China
[c] Institute of Earth Sciences, Chinese Academy of Sciences, Beijing, 100029, China
[d] Bureau of General Affairs, Chinese Academy of Sciences, Beijing, 100864, China
[e] College of Geography and Environmental Sciences, Zhejiang Normal University, Jinhua, 321004, China
[f] Institute of Hydrogeology and Environmental Geology, Chinese Academy of Geological Sciences, Shijiazhuang, 050061, China
[g] Department of Archaeology, Institute of Cultural Heritage, Shandong University, Jinan, 250100, China
[h] School of Geography and Environment, Jiangxi Normal University, Nanchang, 330022, China

ARTICLE INFO

Keywords:
C_4 vegetation
Dune stabilization
Late Quaternary
Desert
China

ABSTRACT

Knowledge of the role of C_4 vegetation expansion in regulating dune stabilization during the late Quaternary is important for understanding the evolution of the environment and climate in the climatically-sensitive margin of the East Asian summer monsoon. However, due to the lack of both reliable vegetation records and chronological control during episodes of dune activity, the relationship between C_4 vegetation expansion and dune stabilization in the deserts of NE China during the late Quaternary remains unclear. Here, we present a new regional compilation of late Quaternary stable carbon isotopic data from organic matter, together with dated records from sub-aerial sedimentary deposits in the region. Our compilation of vegetation development and dune activity in these deserts suggests that C_4 vegetation expansion, with a main contribution from Chenopodiaceae, and a secondary contribution from Poaceae and Cyperaceae, may have played a critical role in dune semi-stabilization with a northwestward trend, from ~13 to 9 ka; and dune stabilization throughout the entire study region, from ~9 to 5 ka. In addition, during the late Holocene, intensified millet cultivation (or overgrazing) and/or climatic deterioration at ~1.5 ka likely caused an increase in C_4 vegetation abundance in the deserts of NE China, which is associated with a dune mobilization episode. In contrast, after ~2.5 ka, decreased vegetation cover and dune mobilization in the Mu Us and Hobq deserts were likely caused by poor land-use practices and historically documented droughts. Overall, C_4 vegetation expansion was the main cause of dune stabilization in these deserts during the late Quaternary.

1. Introduction

Dunes in the deserts of NE China are sensitive to shifts in the desert-grassland boundary (X.P. Yang et al., 2012b; Li and Yang, 2016). A shift from grassland to desert, and the resulting reduction in vegetation cover, may lead to dune mobilization, while the shift from desert to grassland may result in dune stabilization when the vegetation cover increases. Thus, mobile (stable) dunes, indicate a dry (moist) climate, and the corresponding evidence for such changes is preserved in many mid-latitude dune fields, such as eolian sand-paleosol sequences in the deserts of NE China (e.g. Sun et al., 1999, 2006; Lu et al., 2005; Mason et al., 2009; X.P. Yang et al., 2013, 2015b; 2016; Guo et al., 2018a). Consequently, dune activity has been regarded as an important source of information for reconstructing paleoenvironment and paleoclimate at a regional scale, and for predicting future climate changes in arid lands.

Within the deserts of NE China, there has been a substantial research effort to investigate eolian sand-paleosol sequences, with the aim of advancing our understanding of the spatiotemporal variation of dune activity during the late Quaternary. Investigations of well dated sand-paleosol sequences in these deserts reveal that previously unstable dunes began to stabilize at ~10 ka, as suggested by an episode of

* Corresponding author. Institute of Geology and Geophysics, Chinese Academy of Sciences, 19 Bei Tu Cheng Xi Lu, Chaoyang District, Beijing, 100029, China.
** Corresponding author. Institute of Geology and Geophysics, Chinese Academy of Sciences, 19 Bei Tu Cheng Xi Lu, Chaoyang District, Beijing, 100029, China.
E-mail addresses: guolicheng05@mail.iggcas.ac.cn (L. Guo), xiongsf@mail.iggcas.ac.cn (S. Xiong).

https://doi.org/10.1016/j.quaint.2018.10.026
Received 14 May 2018; Received in revised form 19 October 2018; Accepted 21 October 2018
Available online 21 October 2018

Table 1
Factors affecting dune stabilization in the deserts of NE China during the late Quaternary.

Factor	Reference
East Asian monsoon system	(Qiu et al., 1992; Gao et al., 1993; Li et al., 1995; Zhou et al., 1998, 1999, 2001, 2002; Xu et al., 2002b; Jin et al., 2003, 2004, 2010; Huang et al., 2005; Zhou et al., 2005, 2009, 2013; Li and Sun, 2006; Sun et al., 2006; Zhao et al., 2007; Yang et al., 2008; He et al., 2010; Lu et al., 2010; Ma et al., 2011, 2012; Yang and Yue, 2011, 2013; Li et al., 2012; Zhang et al., 2012; Gong et al., 2013; Z.W. Xu et al., 2013b; Yang and Ding, 2013; Yi et al., 2013; Zeng et al., 2013; Zhao et al., 2013; B. Liu et al., 2014, 2015a; J. Liu et al., 2015b; Jia et al., 2015; Guo et al., 2018a,b)
Local climate change	(Wang, 1992; Chen et al., 1993, 1994; Dong and Liu, 1993; Li and Lu, 1996; Xu et al., 2002a; Li et al., 2007)
Global climate change	(Dong et al., 1994; Liu and Hou, 1995; Gao et al., 2001; Li et al., 2002; Han and Sun, 2004; Zhou et al., 2008; Niu et al., 2015)
Northern Hemisphere insolation and/or surface conditions (e.g. effective moisture)	(Dong et al., 1997; Jin et al., 2004, 2010; Lu et al., 2005, 2011, 2012; Mason et al., 2009; Liu et al., 2011, 2013; Liu and Lai, 2012; L.H. Yang et al., 2012a; Yang et al., 2013, 2016)

paleosol and/or weak-paleosol development at that time (Zhao et al., 2007; L.H. Yang et al., 2012a; Yang et al., 2013; Guo et al., 2018a), and possibly before or afterwards (Qiu et al., 1992; Li and Sun et al., 2006; Sun et al., 2006; Mason et al., 2009; Gong et al., 2013; Yi et al., 2013). Subsequently, dunes were remobilized at ~4 ka (X.P. Yang et al., 2015b; Li and Yang, 2016; Guo et al., 2018b), and most recently, were mobilized again at ~2.3 ka (Sun, 2000; Yang et al., 2016). Essentially, late Quaternary dune stabilization in the deserts of NE China was dominated by climate change (Table 1), and active dunes have been used as indicators of arid conditions (Li and Yang, 2016; Guo et al., 2018b) or human activity (Sun, 2000; Yang et al., 2017) in the region. However, the inconsistent timing of the onset of dune stabilization in these deserts, together with our limited knowledge of the mechanisms responsible, hinders our understanding of the relationship between climate change and dune activity during the late Quaternary.

In general, inland dune stabilization is induced by the crossing of a critical threshold caused by an increase in vegetation cover, which results in the decreased mobility of particles transported by the ambient wind regime (Tsoar and Pye, 1987; Tsoar, 2005; Sun and Muhs, 2007). More recent studies in the Mu Us desert show that inland dune stabilization is mainly linked to increased vegetation and weaker winds (Xu et al., 2015a; b). Therefore, vegetation plays a crucial role in dune stabilization, and this is demonstrably true both for parabolic dunes (Reitz et al., 2010; Carlson et al., 2015; Yan and Baas, 2015, 2017; M. Liu et al., 2016b; Guan et al., 2017) and for some deserts (Lubke and Hertling, 2001; Wang et al., 2003). In the case of the deserts of NE China, late Quaternary dune stabilization has been reconstructed from sand-paleosol sequences, and is traditionally linked to changes in the East Asian monsoon system, Northern hemisphere solar radiation, surface characteristics (e.g. effective moisture), and other factors (Table 1). These inferences are based mainly on research on one or more Holocene sand-paleosol sequences, typically using only a few dated records and/or traditional proxies (excluding vegetation records), and they have failed to reveal in detail the onset and causal mechanisms of late Quaternary dune stabilization in the region. In addition, pollen records obtained from lakes in the region (e.g. Xiao et al., 2004; Jiang et al., 2006; Wen et al., 2010, 2017; Zhang et al., 2018) only provide reliable paleovegetation information for the Holocene or the last deglaciation. A recent compilation of late Quaternary stable carbon isotope data from organic matter from the deserts of NE China showed that C_4 vegetation expansion in the Mu Us and Horqin deserts during the early to middle Holocene was associated with an episode of dune stabilization and soil formation (Lu et al., 2012); however, this conclusion was unconfirmed for the Otindag desert. In addition, the conclusions of the study of Lu et al. (2012) are based on a limited dataset for the three deserts, and they highlight the role of temperature and moisture in C_4 vegetation growth, rather than elucidating the linkage of C_4 vegetation and dune activity in the region. Thus, more work is needed to obtain late Quaternary records of the history of vegetation development and dune activity in the region.

Here, we present the results of a study of the spatiotemporal development of vegetation and dune activity in the deserts of NE China during the interval of 25–0 ka, based on a compilation of regional stable carbon isotope data from organic matter, and dated records from subaerial sedimentary deposits. Our results provide the opportunity to investigate the linkage between C_4 vegetation expansion and dune stabilization in the deserts of NE China during the late Quaternary.

2. Regional setting

The deserts of NE China, covering an area of approximately 18,380 km^2, are situated to the east of the north-south-oriented Helan Mountains, on the northern margin of the region of influence of the East Asian summer monsoon (Zhu et al., 1980) (Fig. 1). The dunes in the three northern deserts (Hulun Buir, Horqin and Otindag) and the southern Mu Us desert of NE China are mainly stabilized and semi-stabilized at present, because the current climate is semi-arid. However, the dunes in the Hobq desert are mainly active and semi-stabilized at present, in the semi-arid climate. The degree of aridity in these deserts increases northwestwards, mainly due to a decrease in mean annual precipitation (MAP), from 400 to 500 mm in the southeast to 200 mm in the northwest (Ren et al., 1985). Some 65–75% of the MAP falls from June to September (Liu, 2010). The mean annual pan evaporation (MAE) is 1500–3000 mm in the region.

The modern natural vegetation of these deserts is categorized as temperate steppe and is dominated by grasses (Inner Mongolia-Ningxia Integrated Survey Team, CAS, 1985; Ren et al., 1985; Tang et al., 1999; Pyankov et al., 2000; Wang, 2002, 2007; Wang and Ma, 2016). Needlegrass (*Stipa* sp.), Chinese wild rye (*Aneurolepidium chinense*) and *Cleistogenes squarrosa* are the dominant grasses, and *Artemisia desertorum*, *Agropyron cristatum*, *and Agriophyllum squarrosum* are common. Xerophytic shrubs, mainly *Caragana stenophylla*, *Calligonum*, *Sanina*, *Tamarix*, *Hippophae*, *Salix gordejevii* and *Ulmus pumila*, are also present. Most of the grasses are favored by grazing animals. Additionally, in the region, species of most C_4 vegetation occur in Chenopodiaceae, Poaceae and Cyperaceae (e.g. *Agriophyllum squarrosum*, *Cleistogenes squarrosa* and *Carex pediformis* C. A. Mey) (Pyankov et al., 2000; Wang, 2002, 2007). Several rivers flow through these deserts, including the Yellow River and the Xilamulun, Xiliaohe and Hailar Rivers, which support the irrigation agriculture which enabled the region to become one of the cradles of ancient Chinese civilization (Liu and Chen, 2012; Han, 2015; Guo et al., 2018b). Maize, wheat and millet are grown in the cultivated areas which are widely distributed in riparian zones and in inter-dune lowlands. Accordingly, agro-pastoralism is one of the most distinctive features of the region and has contributed substantially to cultural development and human dispersal.

3. Material and methods

3.1. Sampling

A total of 67 samples for OSL dating were taken from 22 freshly dug

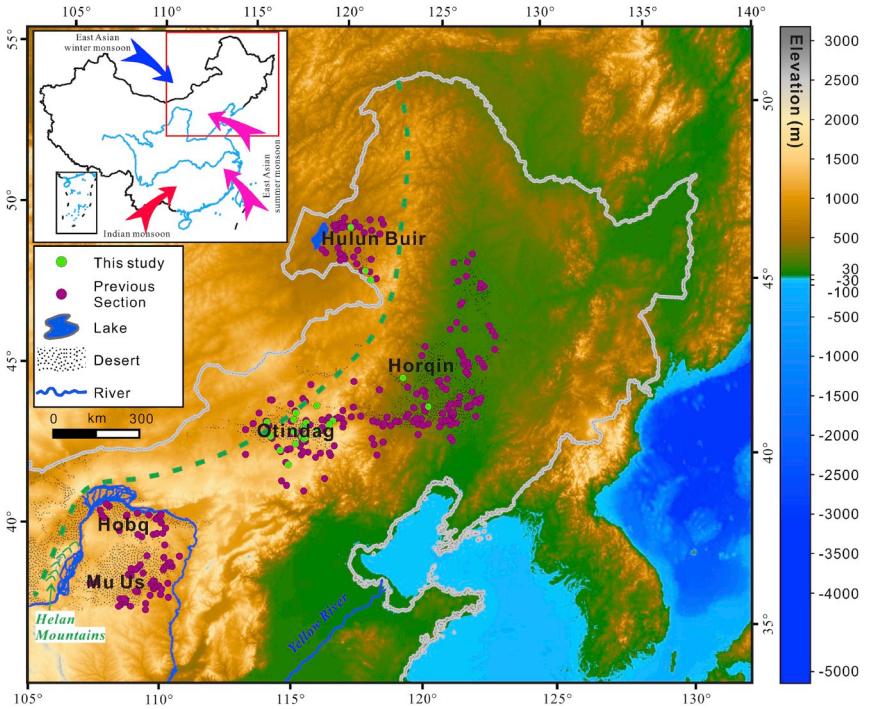

Fig. 1. Distribution of deserts (Hulun Buir, Horqin, Otindag, Hobq and Mu Us) and study sections in NE China. The green dashed line indicates the front of the East Asian summer monsoon. The desert data set is provided by the Environmental and Ecological Science Data Center for West China, National Natural Science Foundation of China, http://westdc.westgis.ac.cn. (For interpretation of the references to colour in this figure legend, the reader is referred to the Web version of this article.)

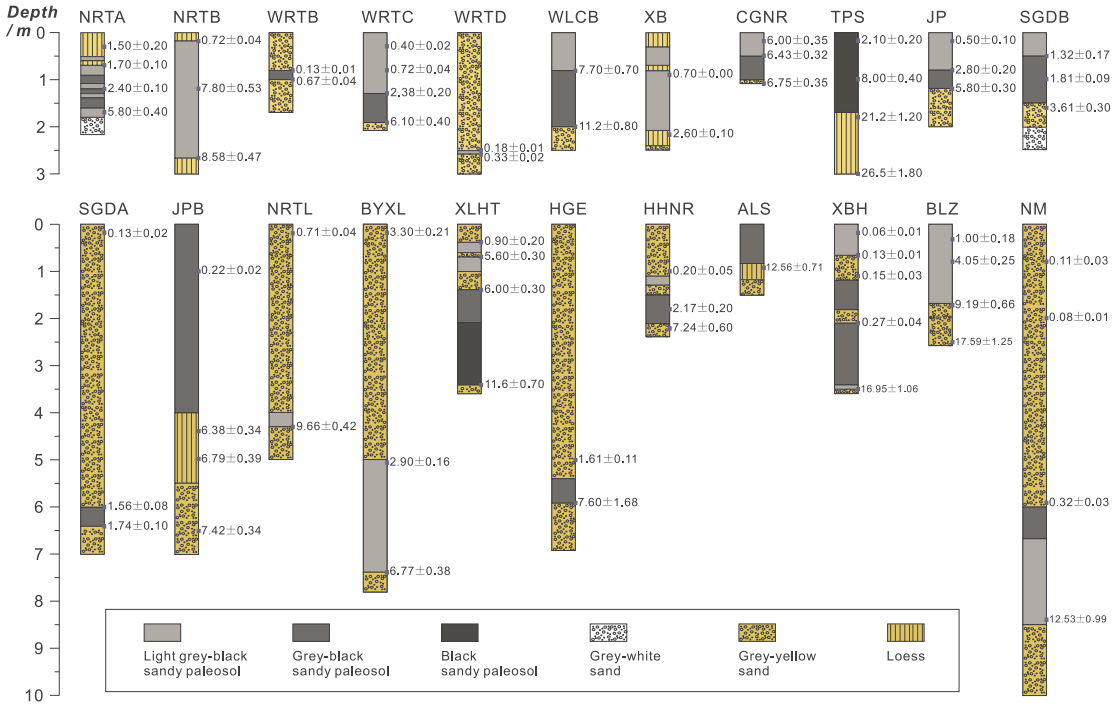

Fig. 2. Stratigraphy, sampling position (blue rectangles) and OSL ages (ka) for the investigated sections in the deserts of NE China. NRTA, NRTB, WRTB, WRTC, WRTD, WLCB, XB, CGNR, TPS, JP, JPB, SGDA, SGDB, NRTL, BYXL, XLHT and HGE are sections in the Otindag desert; HHNR, ALS and XBH (BLZ and NM) are sections in the Hulun Buir desert (Horqin desert). (For interpretation of the references to colour in this figure legend, the reader is referred to the Web version of this article.)

sections in the deserts of NE China (Figs. 1 and 2). At each sampling section, the outer 0.5 m was removed and an aluminum tube was then hammered horizontally into the cleaned face. Then, the sampled material was extracted and sealed in black plastic bags to minimize light exposure and moisture loss (Zhao et al., 2007). In addition, a total of 256 samples were taken at a 10-cm interval from 12 selected sections for analyses of the stable carbon isotope composition ($\delta^{13}C$) of bulk organic matter.

3.2. OSL dating

All OSL samples were prepared and measured under subdued red-light conditions at the Archaeometry Laboratory, University of Science and Technology of China (USTC), Institute of Earth Environments, Chinese Academy of Sciences (IEECAS), and the Institute of Hydrogeology and Environmental Geology, Chinese Academy of Geological Sciences (IHEGCAGS). The sampled material for equivalent dose determination was taken from the central 5-cm interval of the

Table 2
OSL dating results for 67 samples from 22 sections in the deserts of NE China.

Desert	Sample code	Depth (m)	U (ppm)	Th (ppm)	K (%)	Equivalent dose (Gy)	Dose rate (Gy/ka)	Water content (%)	OSL age (ka)	Grain size (μm)	Laboratory
Hulun Buir	XBH-01	0.20	0.51	2.31	2.10	0.16 ± 0.02	2.52 ± 0.13	10 ± 5	0.06 ± 0.01	90–125	IEECAS
Hulun Buir	XBH-02	0.70	0.44	1.96	1.60	0.24 ± 0.01	1.83 ± 0.10	10 ± 5	0.13 ± 0.01	90–125	IEECAS
Hulun Buir	XBH-03	1.10	0.44	2.09	1.91	0.32 ± 0.06	2.10 ± 0.11	10 ± 5	0.15 ± 0.03	90–125	IEECAS
Hulun Buir	XBH-05	2.10	0.45	1.89	1.83	0.55 ± 0.08	1.99 ± 0.11	10 ± 5	0.27 ± 0.04	90–125	IEECAS
Hulun Buir	XBH-07	3.50	0.51	2.53	1.66	31.76 ± 1.01	1.87 ± 0.10	10 ± 5	16.95 ± 1.06	90–125	IEECAS
Hulun Buir	HHNR-02	1.00	0.66	3.13	2.39	0.53 ± 0.12	2.64 ± 0.14	10 ± 5	0.20 ± 0.05	90–125	IEECAS
Hulun Buir	HHNR-04	1.80	0.86	3.82	2.45	6.00 ± 0.45	2.76 ± 0.15	10 ± 5	2.17 ± 0.20	90–125	IEECAS
Hulun Buir	HHNR-05	2.20	0.63	3.02	2.29	18.17 ± 1.13	2.51 ± 0.14	10 ± 5	7.24 ± 0.60	90–125	IEECAS
Hulun Buir	ALS-02	0.90	1.54	7.91	2.27	43.43 ± 0.79	3.46 ± 0.19	10 ± 5	12.56 ± 0.71	4–11	IEECAS
Horqin	NM-01	0.40	0.48	2.21	2.12	0.26 ± 0.06	2.32 ± 0.12	10 ± 5	0.11 ± 0.03	90–125	IEECAS
Horqin	NM-02	2.00	0.45	2.19	2.14	0.17 ± 0.03	2.29 ± 0.12	10 ± 5	0.08 ± 0.01	90–125	IEECAS
Horqin	NM-03	5.90	0.48	2.19	2.05	0.69 ± 0.05	2.15 ± 0.12	10 ± 5	0.32 ± 0.03	90–125	IEECAS
Horqin	NM-05	8.40	0.69	3.43	1.99	27.65 ± 1.55	2.21 ± 0.12	10 ± 5	12.53 ± 0.99	90–125	IEECAS
Horqin	BLZ-01	0.30	0.91	4.35	2.04	2.50 ± 0.42	2.50 ± 0.13	10 ± 5	1.00 ± 0.18	90–125	IEECAS
Horqin	BLZ-02	0.80	0.93	4.34	2.10	10.26 ± 0.33	2.53 ± 0.13	10 ± 5	4.05 ± 0.25	90–125	IEECAS
Horqin	BLZ-04	1.75	0.87	4.29	1.85	20.88 ± 0.99	2.27 ± 0.12	10 ± 5	9.19 ± 0.66	90–125	IEECAS
Horqin	BLZ-05	2.50	0.83	4.04	2.01	41.70 ± 1.96	2.37 ± 0.13	10 ± 5	17.59 ± 1.25	90–125	IEECAS
Otindag	NRTA-01	0.30	0.43	1.73	2.43	4.40 ± 0.43	3.01 ± 0.12	3 ± 1	1.50 ± 0.20	90–125	IHEGCAGS
Otindag	NRTA-02	0.70	0.48	2.05	2.42	5.03 ± 0.29	2.90 ± 0.12	3 ± 1	1.70 ± 0.10	90–125	IHEGCAGS
Otindag	NRTA-03	1.20	0.44	1.95	2.29	6.58 ± 0.30	2.74 ± 0.11	3 ± 1	2.40 ± 0.10	90–125	IHEGCAGS
Otindag	NRTA-05	1.70	0.35	1.42	2.29	15.59 ± 0.93	2.67 ± 0.11	3 ± 1	5.80 ± 0.40	90–125	IHEGCAGS
Otindag	TPS-01	0.20	1.17	6.44	2.08	6.44 ± 0.41	3.07 ± 0.12	3 ± 1	2.10 ± 0.20	4–11	IHEGCAGS
Otindag	TPS-02	1.00	1.19	5.60	2.12	24.39 ± 0.53	3.03 ± 0.12	4.00	8.00 ± 0.40	4–11	IHEGCAGS
Otindag	TPS-03	1.80	1.19	7.00	1.99	66.92 ± 1.41	3.16 ± 0.12	9.20	21.2 ± 1.20	4–11	IHEGCAGS
Otindag	TPS-05	3.00	1.22	6.87	2.04	80.03 ± 4.41	3.02 ± 0.12	3.60	26.5 ± 1.80	4–11	IHEGCAGS
Otindag	XLHT-01	0.40	0.59	2.40	2.54	3.04 ± 0.63	3.25 ± 0.12	3 ± 1	0.90 ± 0.20	90–125	IHEGCAGS
Otindag	XLHT-02	0.70	0.42	2.03	2.55	16.94 ± 0.48	3.02 ± 0.12	3 ± 1	5.60 ± 0.30	90–125	IHEGCAGS
Otindag	XLHT-03	1.40	0.39	2.18	2.49	17.60 ± 0.51	2.95 ± 0.12	3 ± 1	6.00 ± 0.30	90–125	IHEGCAGS
Otindag	XLHT-06	3.40	0.44	1.81	2.28	31.07 ± 1.57	2.68 ± 0.11	3 ± 1	11.6 ± 0.70	90–125	IHEGCAGS
Otindag	JP-01	0.20	0.32	1.36	2.50	1.48 ± 0.40	3.02 ± 0.12	3 ± 1	0.50 ± 0.10	90–125	IHEGCAGS
Otindag	JP-02	0.80	0.46	1.87	2.37	8.24 ± 0.69	2.94 ± 0.12	3 ± 1	2.80 ± 0.20	90–125	IHEGCAGS
Otindag	JP-03	1.20	0.41	1.61	2.41	19.63 ± 0.37	2.91 ± 0.12	3 ± 1	5.80 ± 0.30	90–125	IHEGCAGS
Otindag	XB-02	0.90	1.34	6.03	2.18	2.41 ± 0.13	3.44 ± 0.14	3 ± 1	0.70 ± 0.00	90–125	IHEGCAGS
Otindag	XB-03	2.20	0.57	2.91	2.03	6.99 ± 0.32	2.66 ± 0.11	3 ± 1	2.60 ± 0.10	90–125	IHEGCAGS
Otindag	WLCB-01	0.70	0.45	2.17	2.02	19.87 ± 1.50	2.57 ± 0.10	3 ± 1	7.70 ± 0.70	90–125	IHEGCAGS
Otindag	WLCB-03	2.00	0.44	1.79	2.20	30.28 ± 1.70	2.71 ± 0.11	3 ± 1	11.2 ± 0.80	90–125	IHEGCAGS

Desert	Sample code	Depth (m)	α counting rate (ks)	Stdev	K (%)	Equivalent dose (Gy)	Dose rate (Gy/ka)	Water content (%)	OSL age (ka)	Grain size (μm)	Laboratory
Otindag	WRTB-01	0.80	3.21	0.10	2.26	0.37 ± 0.038	2.76 ± 0.09	4.02	0.13 ± 0.01	150–250	USTC
Otindag	WRTB-02	1.00	2.85	0.09	1.83	1.60 ± 0.08	2.39 ± 0.08	3.34	0.67 ± 0.04	150–250	USTC
Otindag	WRTC-01	0.30	3.74	0.10	2.57	1.29 ± 0.07	3.23 ± 0.11	2.79	0.40 ± 0.02	150–250	USTC
Otindag	WRTC-02	0.80	2.87	0.09	2.26	2.06 ± 0.08	2.86 ± 0.09	3.12	0.72 ± 0.04	150–250	USTC
Otindag	WRTC-03	1.30	2.74	0.09	2.39	6.94 ± 0.54	2.91 ± 0.10	9.53	2.38 ± 0.20	150–250	USTC
Otindag	WRTC-04	1.90	2.30	0.08	2.29	17.32 ± 0.97	2.84 ± 0.09	4.81	6.10 ± 0.40	150–250	USTC
Otindag	WRTD-01	2.50	2.37	0.08	2.34	0.56 ± 0.031	2.98 ± 0.10	1.22	0.18 ± 0.01	150–250	USTC
Otindag	WRTD-02	2.60	2.28	0.08	2.36	0.96 ± 0.06	2.93 ± 0.10	1.38	0.33 ± 0.02	150–250	USTC
Otindag	NRTL-01	0.20	2.63	0.09	1.80	1.68 ± 0.087	2.35 ± 0.07	2.00	0.71 ± 0.04	150–250	USTC
Otindag	NRTL-02	4.30	2.60	0.09	1.62	20.58 ± 0.62	2.13 ± 0.07	2.77	9.66 ± 0.42	150–250	USTC
Otindag	SGDB-01	0.50	2.41	0.02	2.25	3.61 ± 0.44	2.75 ± 0.09	5.12	1.32 ± 0.17	150–250	USTC
Otindag	SGDB-02	1.00	2.14	0.07	2.18	4.85 ± 0.18	2.69 ± 0.09	4.65	1.81 ± 0.09	150–250	USTC
Otindag	SGDB-03	1.60	3.27	0.09	2.24	9.89 ± 0.77	2.74 ± 0.09	3.71	3.61 ± 0.30	150–250	USTC
Otindag	SGDA-01	0.20	2.50	0.08	1.95	0.32 ± 0.05	2.49 ± 0.08	1.10	0.13 ± 0.02	150–250	USTC
Otindag	SGDA-02	6.00	2.48	0.10	2.10	4.15 ± 0.17	2.67 ± 0.09	5.45	1.56 ± 0.08	150–250	USTC
Otindag	SGDA-03	6.40	2.70	0.11	2.09	4.60 ± 0.20	2.64 ± 0.09	2.07	1.74 ± 0.10	150–250	USTC
Otindag	NRTB-01	0.20	2.07	0.10	2.14	1.90 ± 0.09	2.64 ± 0.09	3.29	0.72 ± 0.04	150–250	USTC
Otindag	NRTB-02	1.20	2.17	0.10	2.14	20.58 ± 1.21	2.64 ± 0.09	4.05	7.8 0 ± 0.53	150–250	USTC
Otindag	NRTB-03	2.70	3.05	0.12	2.09	22.06 ± 0.95	2.57 ± 0.09	2.57	8.58 ± 0.47	150–250	USTC
Otindag	BYXL-01	0.20	2.71	0.12	1.91	8.04 ± 0.44	2.43 ± 0.08	1.52	3.30 ± 0.21	150–250	USTC
Otindag	BYXL-02	5.10	2.84	0.12	2.04	7.64 ± 0.33	2.63 ± 0.08	3.56	2.90 ± 0.16	150–250	USTC
Otindag	BYXL-03	7.40	2.35	0.11	1.92	16.07 ± 0.74	2.37 ± 0.08	6.81	6.77 ± 0.38	150–250	USTC
Otindag	CGNR-03	0.20	3.83	0.01	2.31	17.62 ± 0.85	2.95 ± 0.09	6.50	6 .00 ± 0.35	150–250	USTC
Otindag	CGNR-04	0.50	3.86	0.11	2.31	18.92 ± 0.73	2.94 ± 0.09	6.46	6.43 ± 0.32	150–250	USTC
Otindag	CGNR-05	1.10	3.53	0.09	2.38	19.73 ± 0.79	2.92 ± 0.10	7.69	6.75 ± 0.35	150–250	USTC
Otindag	HGE-01	5.00	2.90	0.08	2.43	4.93 ± 0.31	3.06 ± 0.10	1.74	1.61 ± 0.11	150–250	USTC
Otindag	HGE-02	5.90	4.08	0.10	2.37	23.69 ± 5.17	3.12 ± 0.10	3.56	7.60 ± 1.68	150–250	USTC
Otindag	JPB-01	1.00	2.09	0.07	2.23	0.61 ± 0.053	2.78 ± 0.09	1.20	0.22 ± 0.02	150–250	USTC
Otindag	JPB-02	4.40	2.05	0.09	2.32	17.36 ± 0.68	2.71 ± 0.10	5.45	6.38 ± 0.34	150–250	USTC
Otindag	JPB-03	5.00	0.00	0.00	2.27	16.76 ± 0.74	2.47 ± 0.09	2.00	6.79 ± 0.39	150–250	USTC
Otindag	JPB-04	6.50	2.03	0.09	2.12	19.61 ± 0.63	2.64 ± 0.09	1.11	7.42 ± 0.34	150–250	USTC

sampling tube, and the remaining material from both ends was used for environmental dose rate determination.

Samples for equivalent dose determination were first digested in 30% H_2O_2 and 30% HCl at room temperature to remove organic material and carbonates, respectively. The samples were then washed to near-neutral pH (the pH ranged from 5 to 7) with distilled water, followed by settling and sieving to isolate the desired 4–11, 90–125 and 150–250 μm grain-size fractions for the various sections (Table 2), using the procedure of Guo et al. (2016). It is important to note that the grain-size distribution of the sediments, together with the natural alpha, beta, gamma and cosmic radioactivity, plays a crucial role in assessing the applicability of OSL dating (Aitken, 1998).

For the 90–125 or 150–250 μm grain-size fractions, heavy liquid flotation (sodium polytungstate) was used to extract coarse quartz grains which were then rinsed and treated with 40% HF at room temperature for 1 h to dissolve feldspar and etch the outer alpha-irradiated surface layer. For the 4–11 μm fraction, 30% HF was added at room temperature for 5–7 days to extract the fine quartz grains. All quartz grains were finally treated with HCl (10%) to dissolve insoluble fluorides produced during the previous steps. In addition, the purity of the quartz grains was assessed by drying at 45 °C and then testing with infrared stimulated luminescence, prior to measurement. Finally, the purified fine and coarse quartz grains were mounted on stainless steel discs using acetone and silicon-based adhesive, respectively.

All equivalent dose measurements were performed at the three TL/OSL dating laboratories using an automated Risø TL/OSL-DA-20 reader system (USTC) or an automated Daybreak 2200 OSL reader system (IEECAS and IHEGCAGS) equipped with a $^{90}Sr/^{90}Y$ beta source and blue and infrared light excitation units. The blue LEDs (470 ± 5 nm) were applied at 125 °C for 200 s at IECEA, for 40 s at USTC, and for 100 s at IHEGCAGS. The stimulated quartz OSL signals were detected using an EMI 9235QA photomultiplier coupled in front with one 7.5-mm-thick U-340 or two 3-mm-thick glass filters. As suggested by Wintle and Murray (2006), the single-aliquot regenerative-dose (SAR) protocol was used to measure the equivalent dose. Respective preheat temperatures of 260 °C (10 s) and 220 °C (10 s) were used for natural/regenerative dose and test dose responses. We used 6–40 aliquots for each sample for equivalent dose determination.

According to the OSL age equation suggested by Aitken (1998), the environmental dose rate was derived from the concentrations of radioactive elements (U, Th, K), using the dose-rate conversion factors described in Guérin et al. (2011) and considering the effects of moisture content and cosmic radioactivity (Aitken, 1998; Prescott and Hutton, 1994). At USTC, the environmental dose rate was measured using thick source alpha counting to calculate the contribution of the U and Th decay chains to the environmental dose rate; X-ray fluorescence was used to measure the K concentration (Fan et al., 2015). However, at IEECAS and IHEGCAGS, the concentrations of U and Th were measured using inductively coupled plasma mass spectrometry, and X-ray fluorescence was used to determine the K concentration (Kang et al., 2015).

Aitken (1998) suggested that water in the interstices of the sediment grains can absorb part of the alpha, beta, and gamma energy. Thus, overlooking the effects of moisture can lead to an underestimation of the OSL age. In practice, the water content may change during the entire interval of burial and therefore it is difficult to estimate the past water content. However, a water content of 10% is regarded as an appropriate average value for the entire interval of burial (Aitken, 1998), and can be used as a conversion factor for calculating the dose rate. In addition, the measured water content of the sampled material at both ends of the sampling tube is generally assumed to represent the average wetness during the entire interval of burial (Fan et al., 2015).

In this study, for the samples from the Horqin and Hulun Buir deserts, a water content of 10% was used to calculate the dose rate; for the samples from the Otindag desert the measured water content was used. A water content of 3%, close to the average measured water content value (3.86%) of some of the samples from the Otindag desert, was used to calculate the dose rate of other samples from this desert. The contribution of cosmic radioactivity to the dose rate was calculated as a function of depth, as suggested by Prescott and Hutton (1994), considering the latitude, longitude and altitude of the samples.

3.3. $\delta^{13}C$ analysis of bulk organic matter

After removal of modern rootlets, samples (~3 g) were treated with 10% HCl at ~25 °C for 24 h to remove inorganic carbonate, followed by washing to near-neutral pH with distilled water, and then drying to 50 °C. Then, about 20 mg of dried sample was combusted for 4 h at 850 °C in evacuated sealed quartz tubes in the presence of silver foil and cupric oxide. The carbon isotopic composition of the evolved CO_2 was measured using a MAT-253 gas mass spectrometer with a dual inlet system at the Institute of Geology and Geophysics, Chinese Academy of Sciences; the total organic carbon content (TOC) of the samples was determined simultaneously. The organic carbon is derived predominantly from terrestrial higher vegetation, because hydrophytes would not be able to survive given the high MAE (1500–3000 mm) in the region. Thus, the measured high values of the stable carbon isotope composition of organic matter ($\delta^{13}C_{org}$) relate mainly to the C_4 biomass (Rao et al., 2008; Lu et al., 2012).

We also assessed the role of meteorological factors on the $\delta^{13}C_{org}$ values by comprehensively investigating the $\delta^{13}C_{org}$ values of a large number of topsoil samples from sites in the studied deserts and adjacent regions (Fig. 3; Wang et al., 2013; Chen et al., 2015; L. Liu et al., 2016a). Contour maps of the meteorological factors were generated using ArcGIS 10.2 together with the Kriging interpolation tool, using long-term (1961–2010) climate data.

4. Results

4.1. Late Quaternary dated records of mobile and stable states in the deserts of NE China

The OSL dating results for the quartz grains from the 67 samples are summarized in Table 2 and presented in Fig. 2. A tight normal distribution of equivalent doses for representative samples is evident (Fig. 4), as is also shown by the luminescence characteristics of the TQ and MTG sections measured under duplicated conditions at IEECAS (Guo et al., 2018a). This suggests that the samples were well bleached prior to deposition and can be used to determine the equivalent dose.

As suggested by Li and Yang (2016), a compilation of dated late Quaternary records from sub-aerial sedimentary deposits in deserts enables us to characterize the spatiotemporal development of episodes of dune activity, and hence achieve an improved understanding of the associated environmental changes and effects. Thus, we made a detailed compilation of dated records, spanning the interval of 25–0 ka, from sub-aerial sedimentary deposits in this region. It is widely believed that abundant EASM precipitation favors plant growth and the development of paleosols and lakes, whereas a deficit of EASM precipitation results in dune reactivation; moreover, reactivated dunes are the major source of loess deposits in the margin of the deserts of NE China (Guo et al., 2018b). Paleosols and lacustrine and peat deposits are the sources of dated records indicating a stable dune state, while eolian sand and loess are the sources of dated records for a mobile dune state. All published actual ages were selected using the three criteria described in Guo et al. (2018b): (i) All selected published actual ages were determined by radiocarbon or luminescence methods; (ii) the ages were in stratigraphic order; (iii) we selected a single dated record when multiple ages or similar ages were measured from the same layer at a site. Finally, uncalibrated radiocarbon ages were calibrated to calendar years using the Calib Rev 7.0.4 radiocarbon age calibration program (Stuiver and Reimer, 1993) with the IntCal13 curve (Reimer et al., 2013). The data set consists of 1018 dated records, including our 64 new OSL dates, together with 811 published dated records from the

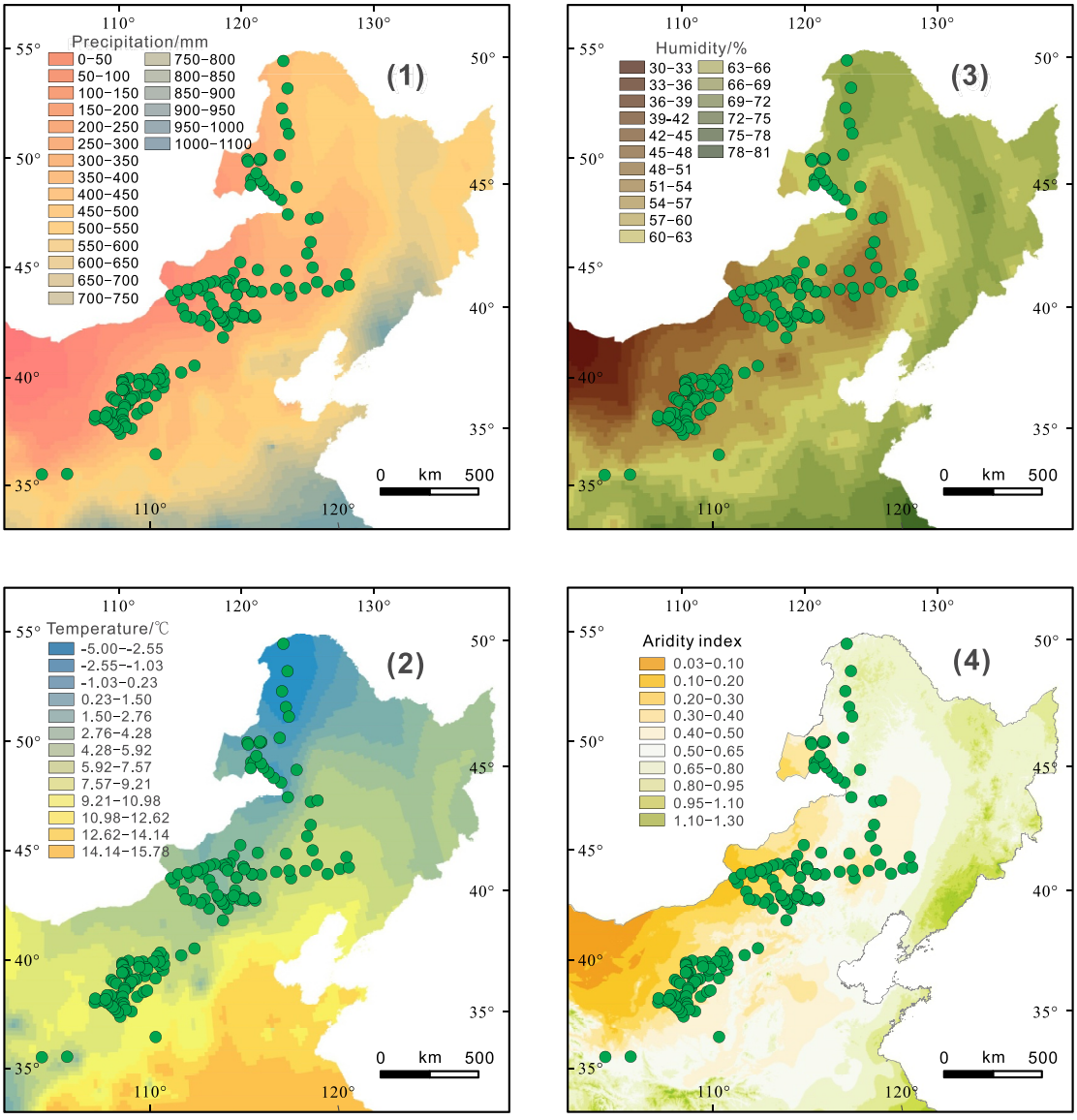

Fig. 3. Topsoil sites in NE China, together with modern mean annual precipitation (MAP, 1), and mean annual temperature (MAT, 2), humidity (3) and Aridity index (4, Aridity index = MAP/MAE, suggested by UNEP (1997)) over 50 y (1961–2010). Long-term climate data are provided by the National Meteorological Information Center of China Meteorological Administration. The information on topsoil sites in the deserts of NE China and adjacent regions is from Wang et al. (2013), Chen et al. (2015) and L. Liu et al. (2016a).

study of Guo et al. (2018b) for the interval from 12 to 0 ka, and 143 newly-compiled dated records for the interval from 25 to 12 ka. Within the data set, there are 473 records of dune mobility and 545 records of dune stability. Detailed information on these dated records is listed in Table 3.

The spatiotemporal distribution of states of dune stability and mobility in the deserts of NE China during the late Quaternary is shown in Figs. 5 and 6 using respective bin widths of 200 and 1000 y. Dated records during some intervals (e.g. from 25 to 18 ka, 9–6 ka, and 4–0 ka) are excluded. The records for the five deserts show a similar spatiotemporal distribution. The synthesis reveals that for the interval from ~18 to 13 ka, the numbers of dated records indicating mobile dune states are relatively low but with an increasing trend; for ~13–9 ka, relatively high values are maintained; for ~9–4 ka the values decrease, with a minimum at ~4.5 ka; and from ~4 ka the values gradually increase. For stable dune states, for the interval from ~18 to 13 ka there are very few dated records; for ~13–9 ka the number of records increases; for ~9–5 ka there are a relatively large number of records; for ~5–4 ka there is minimum number of records; and since ~4 ka the numbers are relatively high and they fluctuate within a large range.

In addition, for the Otindag desert, the numbers of dated records for stable states first increase at ~12 ka and then lag the other deserts by ~1 kyr. In the deserts of NE China, the dated records indicate a substantial increase in mobile and stable dune states at ~1.5 ka; whereas for the Mu Us and Hobq deserts there is a substantial increase in the number of records of mobile dune states at ~2.5 ka, with few records subsequently.

4.2. Changes in stacked $\delta^{13}C_{org}$ and TOC values during the late Quaternary

The stacked $\delta^{13}C_{org}$ and TOC values are plotted in Fig. 7. The $\delta^{13}C_{org}$ and TOC values are low from ~25 to 13 ka; they increase from ~13 to 9 ka; they are relatively high during ~9–5 ka; they decrease substantially from ~5.0 to 1.5 ka; and thereafter they increase substantially and remain relatively high.

Estimates of C_4 biomass from stacked $\delta^{13}C_{org}$ values, using the methods described in S.L. Yang et al. (2015a) and Guo et al. (2018a), indicate values of C_4 biomass of less than ~10% from ~25 to 13 ka;

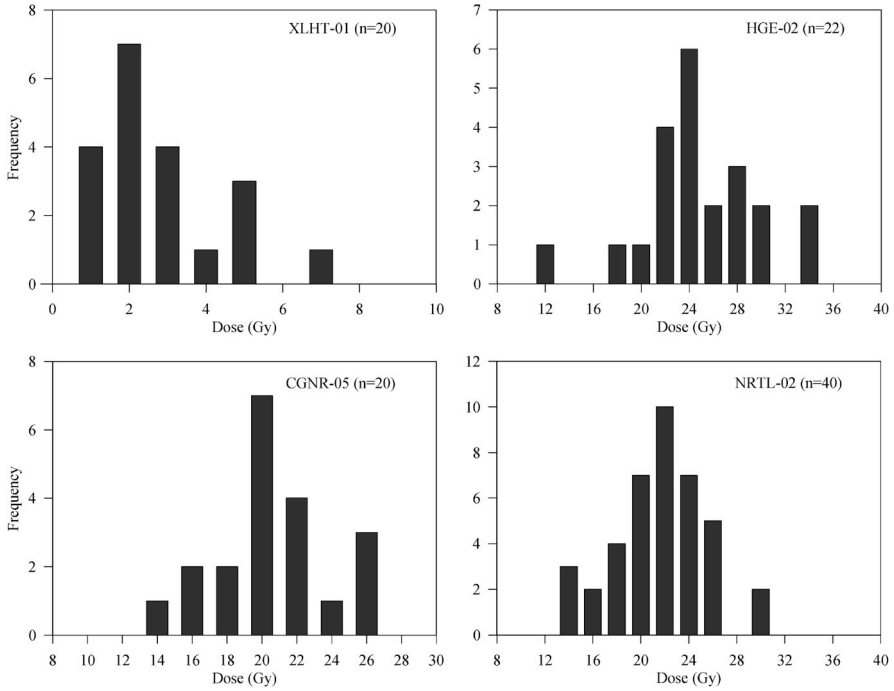

Fig. 4. Histograms of equivalent dose distribution for selected representative samples.

Table 3
Distribution of luminescence and radiocarbon ages for the deserts of NE China.

Region	Luminescence dates			Radiocarbon dates	Total	Number of sites
	OSL	IRSL	TL			
Hulun Buir	102	–	–	21	123	39
Horqin	246	–	2	89	337	117
Otindag	250	–	2	43	295	88
Hobq	31	–	–	8	39	18
Mu Us	122	2	12	88	224	67
Total	751	2	16	249	1018	329

Note: '-' indicates no data.
Abbreviations: OSL, Optically stimulated luminescence; IRSL, Infrared-stimulated luminescence; TL, Thermoluminescence.

however, after ~ 9 ka the values exceed ~20%, with a maximum value of ~40%. Thus, we speculate that the amplitude of variation of C_4 plant biomass was up to ~300%. However, the minimum $\delta^{13}C_{org}$ value of −25‰ for all samples shows that the C_3 plant biomass was maintained throughout the late Quaternary. In addition, the TOC values increase from 0 to 0.5% during ~25–13 ka, and from 1.0 to 1.5% during ~9–0 ka, with a minimum amplitude of increase of ~200%.

4.3. Factors controlling $\delta^{13}C_{org}$ values of topsoils in the deserts of NE China

A comprehensive investigation of the $\delta^{13}C_{org}$ values of topsoils at a small regional scale in the deserts of NE China revealed a negative relationship between precipitation and $\delta^{13}C_{org}$ and a strong positive relationship between $\delta^{13}C_{org}$ and temperature (Wang et al., 2013; Chen et al., 2015). However, other results from sand-paleosol sequences from the region indicated that the distribution of C_4 vegetation was controlled by the East Asian summer monsoon precipitation (Guo et al., 2018a), or by the effective moisture (Lu et al., 2012). A spatial comparison of meteorological variables and $\delta^{13}C_{org}$ values of topsoils in the deserts of NE China and adjacent regions demonstrates that it is impossible to separate the roles of temperature and precipitation as controls of $\delta^{13}C_{org}$ because of the seasonal synchrony of rainfall and temperature in the East Asian monsoon region (Fig. 8a–c).

In practice, the degree of aridity is likely to control changes in the $\delta^{13}C_{org}$ values of topsoils in the deserts of NE China and adjacent regions. This is because the Aridity index (Aridity index = MAP/MAE), suggested by UNEP (1997), varies inversely with $\delta^{13}C_{org}$, and fluctuates within a relatively large range when $\delta^{13}C_{org}$ exceeds −22‰ (Fig. 8d). The Aridity index is an aggregated proxy of temperature, precipitation and seasonality, and therefore it provides a convenient means of estimating the C_3/C_4 relative abundance based on the $\delta^{13}C_{org}$ values of sections in the deserts of NE China during the late Quaternary.

5. Discussion

5.1. Spatiotemporal changes in dune semi-stabilization in the deserts of NE China from ~13 to 9 ka

Previous research on dune activity in the deserts of NE China from ~13 to 9 ka has focused mainly on dune mobilization, and relatively little attention has been paid to dune stabilization (Lu et al., 2012; Yi et al., 2013; Xu et al., 2015a; Li and Yang, 2016). The reasons for this are the relative abundance of dated records indicating stable dune states from sand-paleosol sequences for the late Quaternary (Yi et al., 2013; Xu et al., 2015a); and the fact that dune stabilization, traditionally inferred by an episode of paleosol (or weak-paleosol) development, is dated back to the early Holocene (Qiu et al., 1992; Li and Sun et al., 2006; Sun et al., 2006; Zhao et al., 2007; L.H. Yang et al., 2012a; Gong et al., 2013; Yi et al., 2013; Yang et al., 2013; Guo et al., 2018a).

Our spatiotemporal record of dune activity in the deserts of NE China during the late Quaternary can be divided into four stages (Fig. 9a): dune mobilization (~25–13 ka), dune semi-stabilization (~13–9 ka), dune stabilization and paleosol development (~9–5 ka), and dune re-mobilization (~5 ka onwards). However, during the late Pleistocene, the Otindag desert dunes began to stabilize at ~12 ka with a lag of ~1 kyr relative to other deserts in NE China, suggesting that dune semi-stabilization from ~13 to 9 ka was asynchronous in the region, with a trend of increasing lag of semi-stabilization towards the northwest (Figs. 5 and 6).

Previous work has revealed that inland dune activity is linked

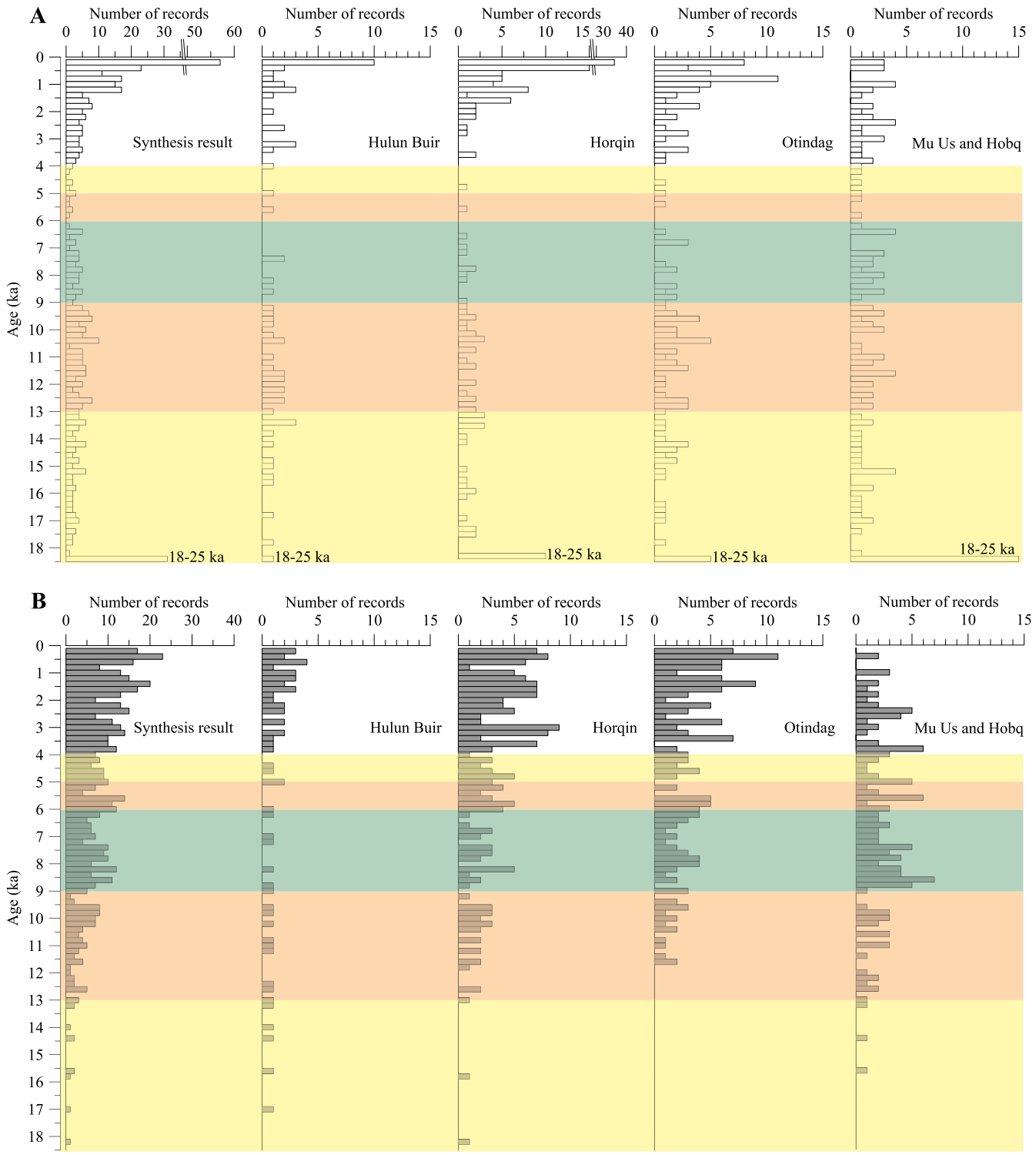

Fig. 5. Histogram of dated records for mobile (A) and stable (B) dune states in the deserts of NE China over the last 25 kyr. Humid periods are shown by green rectangles and dry (driest) periods are shown by light orange (yellow) rectangles. (For interpretation of the references to colour in this figure legend, the reader is referred to the Web version of this article.)

mainly to the supply, transportation and preservation of sand (Roskin et al., 2011; X.P. Yang et al., 2012b; Leighton et al., 2014; Xu et al., 2015a). Therefore, the sand source, winds, landforms and local climate (including vegetation) strongly affect dune stabilization (Pye and Tsoar, 2009; X.P. Yang et al., 2012b). Nevertheless, inland dune stabilization is also affected by local geological processes, such as the retreat of the Laurentide Ice Sheet in North America during the late deglaciation (Dallimore et al., 1997; Wolfe et al., 2004; Bateman and Murton, 2006; Munyikwa et al., 2017). Thus, the various influencing factors need to be considered in the context of the local geographical background. Xu et al. (2015a) suggested that in the Mu Us desert during the Last Glacial Maximum, the continuous recycling of dunes driven by strong wind activity, as well as the sufficient but not abundant sand supply, led to the poor preservation of dunes given the minimal vegetation cover and dry conditions. Subsequently, during the last deglaciation, dune mobilization in the Mu Us desert was continuously enhanced due to the

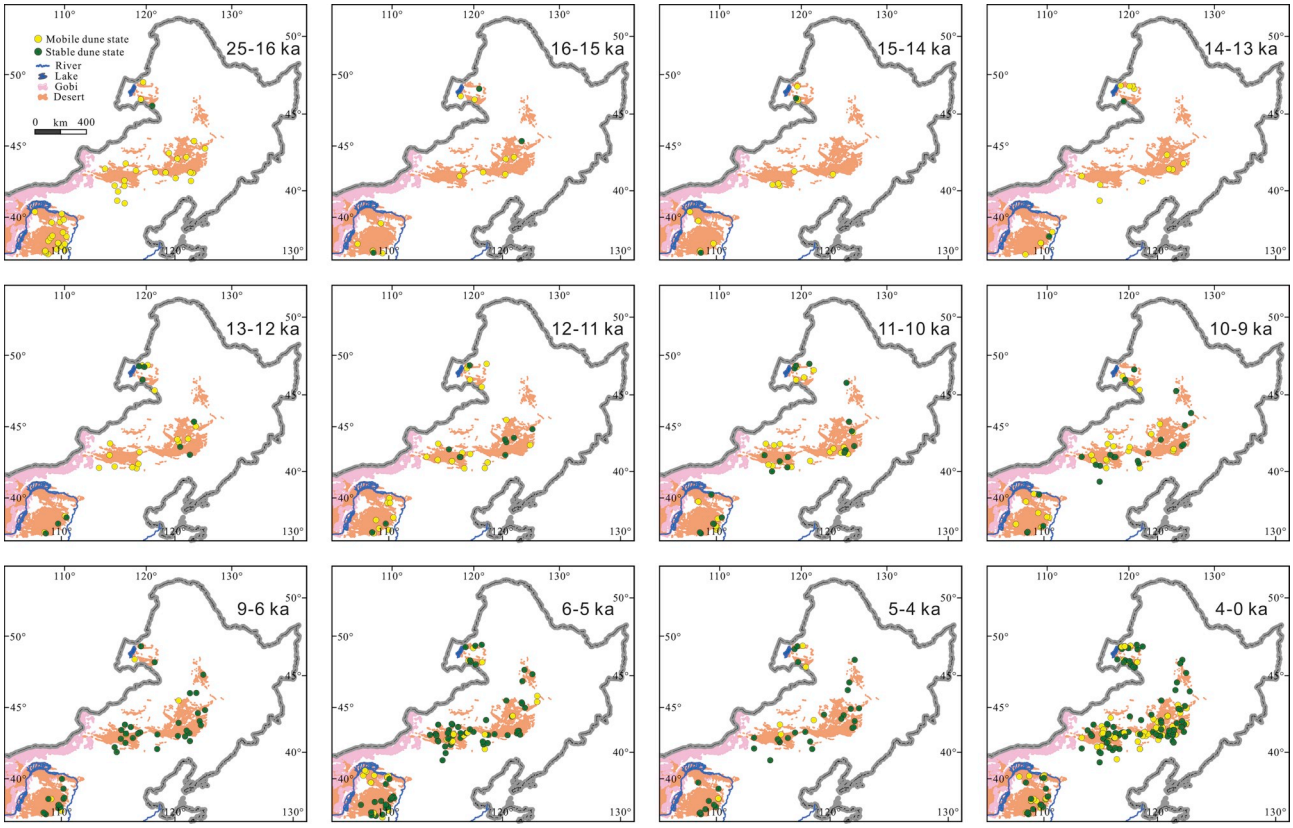

Fig. 6. Spatiotemporal distribution of late Quaternary dated records of sub-aerial sedimentary deposits in the deserts of NE China. These dated records of mobile and stable dune states reveal trends in late Quaternary dune activity in these deserts. The extent of the deserts in all maps only reflects their modern status.

reduced wind strength, as well as by the possibly increased sediment influx derived from regional permafrost degradation and increased fluvial activity, and the occurrence of localized vegetation patches, as the climate ameliorated. The pattern of dune stabilization in the deserts of NE China indicated by our dated records (Figs. 5 and 6) shows a similar pattern with that in the study of Xu et al. (2015a) during the late Quaternary.

The number of dated records for stable dune states increases

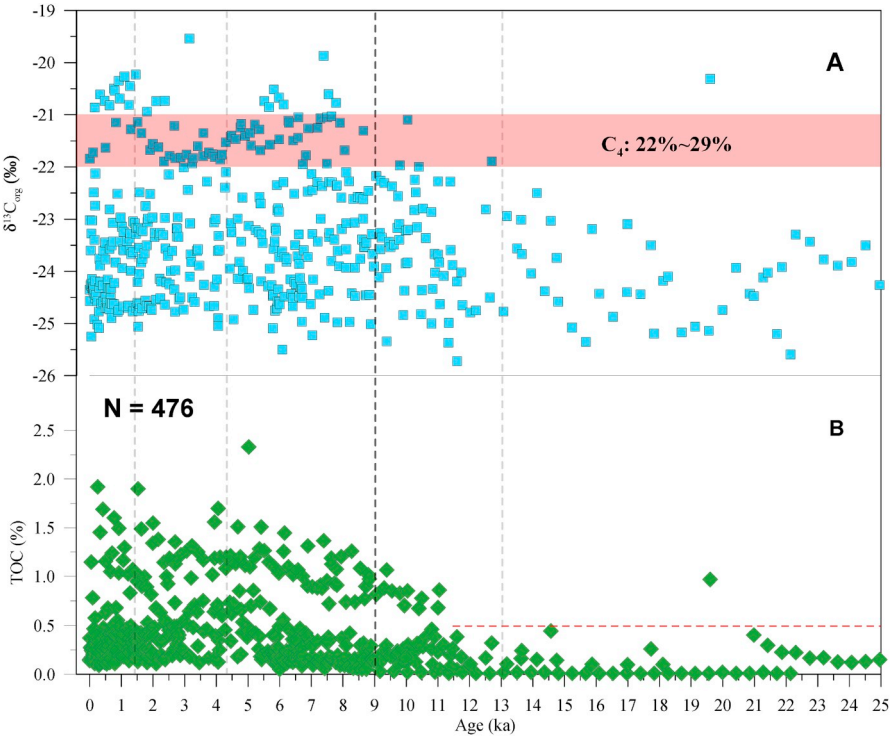

Fig. 7. Stacked $\delta^{13}C_{org}$ (A) and TOC (B) records for the last 25 kyr in the deserts of NE China. The data comprise 256 new records of both proxies from 12 selected sections in the region, together with a compilation of 220 published records from 23 sections (Lu et al., 2005, 2012; 2013; Mason et al., 2009; Guo et al., 2018a) compiled by this study. Estimates of C_4 biomass are based on the method described in S.L. Yang et al. (2015a) and Guo et al. (2018a).

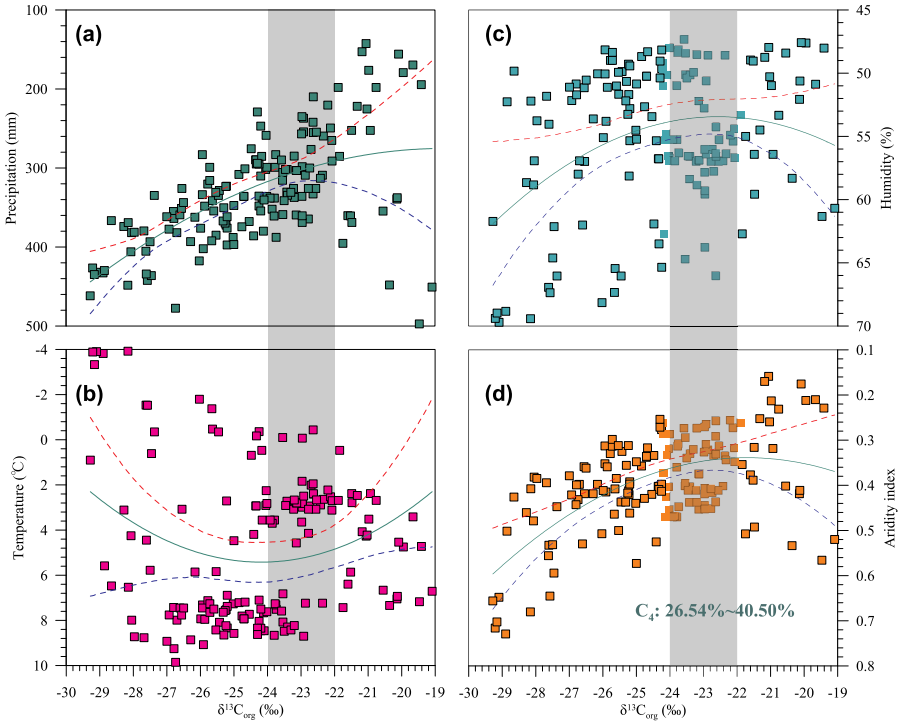

Fig. 8. Relationship between the $\delta^{13}C_{org}$ values of topsoils and modern MAP (a), MAT (b), humidity (c) and Aridity index (d). Estimates of C_4 biomass are based on the method described in S.L. Yang et al. (2015a) and Guo et al. (2018a). The $\delta^{13}C_{org}$ values of topsoils in NE China are from Wang et al. (2013), Chen et al. (2015) and L. Liu et al. (2016a). Fit line is shown by green solid line and upper (lower) level of the confidence is shown by red (blue) dotted line. (For interpretation of the references to colour in this figure legend, the reader is referred to the Web version of this article.)

substantially for the interval from ~13 to 9 ka, which implies that the climate ameliorated during this interval; this is supported by the continuous expansion of localized vegetation indicated by our stacked $\delta^{13}C_{org}$ and TOC values (Figs. 7 and 9b) and by global records (Fig. 9c–e). Localized vegetation development would have anchored the dunes during the last deglaciation (Xu et al., 2015a), which is demonstrated by the role of vegetation in the formation of parabolic dunes (Reitz et al., 2010; Carlson et al., 2015; Yan, and Baas, 2015, 2017; M. Liu et al., 2016b; Guan et al., 2017). In addition, the delayed dune semi-stabilization from ~13 to 9 ka in the northwestern part of the study area was likely the result of the greater aridity. This inference is supported by the contour maps of the Aridity index which indicate drier conditions in the Otindag desert (Fig. 3), which would have adversely affected vegetation growth and may explain the observed lag of ~1 kyr compared to the other deserts. Thus, localized vegetation development, controlled by the degree of aridity, evidently played a crucial role in the northwestward-trend of dune semi-stabilization in the deserts of NE China from ~13 to 9 ka.

5.2. C_4 vegetation expansion in the deserts of NE China from ~13 to 5 ka

Our new compilation of records of dune activity and vegetation suggest that the local vegetation was the cause of dune semi-stabilization (~13–9 ka) and stabilization (~9–5 ka) in the deserts of NE China during the late Quaternary (Fig. 9a and b). The episode of dune stabilization and soil formation during the early to middle Holocene was tentatively interpreted as an evidence for C_4 vegetation expansion (Lu et al., 2012). However, the processes by which the vegetation anchors the dunes in the region remain to be thoroughly understood, which limits our understanding of the fundamental mechanisms of dune stabilization in these deserts.

Studies of the $\delta^{13}C_{org}$ values of modern plants and surface soils at a global scale indicate a close relationship between MAT and C_4 vegetation abundance, and a significant positive correlation between MAP and C_3 vegetation abundance (Rao et al., 2017). However, the $\delta^{13}C_{org}$ values of topsoils in the deserts of NE China show that the C_3/C_4 relative vegetation abundance is strongly influenced by the degree of aridity (Fig. 8d). When $\delta^{13}C_{org}$ is less than −22‰, the $\delta^{13}C_{org}$ values of topsoils and Aridity index in these deserts are negatively correlated; however, there is no close relationship between the $\delta^{13}C_{org}$ values of topsoils and Aridity index when $\delta^{13}C_{org}$ exceeds −22‰, probably due to the ability of localized C_4 vegetation to tolerate a wide range of humidity and aridity conditions. Thus, from the Last Glacial Maximum to the Holocene, as the global climate ameliorated, the C_3/C_4 relative abundance in the deserts of NE China decreased synchronously as a consequence of decreased aridity, as indicated by the Aridity index (Fig. 9c–e), and at the same time the East Asian monsoon rainfall belt migrated northwestwards (S.L. Yang et al., 2015a). In addition, our stacked $\delta^{13}C_{org}$ and TOC records show that the C_3/C_4 relative abundance decreased gradually from ~13 to 9 ka and maintained a relatively low value during ~9–5 ka, in agreement with our evidence for dune semi-stabilization and stabilization, respectively, during these two intervals (Fig. 9a).

Consequently, considering both the contribution of C_3 biomass to the vegetation since the Last Glacial Maximum, and the increased representation of C_4 biomass, we speculate that the reason for dune stabilization during ~13–5 ka was mainly due to the pronounced increase in C_4 vegetation abundance, with a secondary contribution from the expansion of C_3 vegetation. Although dune stabilization episodes in the study region, and in deserts in several low latitude regions, occurred synchronously during the early Holocene (Munyikwa, 2005), C_3 vegetation expansion likely played the dominant role in dune stabilization in low latitudes during the Holocene, due to the fact that the increased precipitation (Huang et al., 2001; Rao et al., 2017) and atmospheric CO_2 concentration (Damsté et al., 2011) probably limited the expansion of C_4 vegetation and conversely increased the C_3 vegetation abundance.

Comparison of pollen records form lake sediments during the interval of ~13–5 ka (Jiang et al., 2006; Wen et al., 2010, 2017; Zhang et al., 2018), and the composition of the modern vegetation of the deserts of NE China and the adjacent regions (Inner Mongolia-Ningxia Integrated Survey Team, CAS, 1985; Ren et al., 1985; Tang et al., 1999; Pyankov et al., 2000; Wang, 2002, 2007; Wang and Ma, 2016), reveals that in both cases *Artemisia* is the dominant herb and is a major component of the C_3 vegetation. In addition, Chenopodiaceae comprise ~50% of the C_4 vegetation, with a secondary contribution from Poaceae and Cyperaceae. For example, as one of the pioneer annual C_4

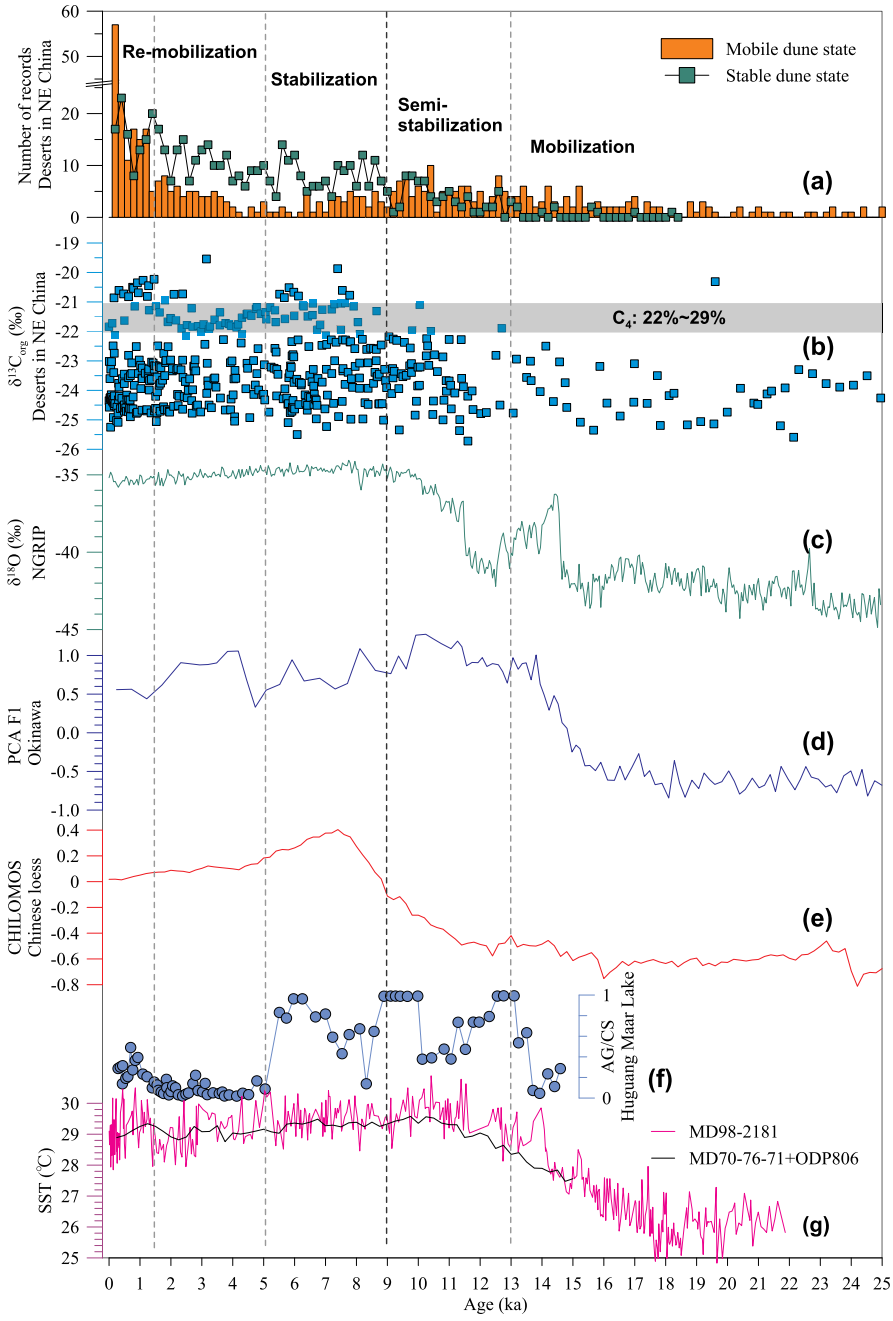

Fig. 9. Late Quaternary dated records and stacked $\delta^{13}C_{org}$ values of sub-aerial sedimentary deposits (a and b, respectively, this study) in the deserts of NE China compared with other paleoclimatic records. (c) NGRIP ice-core $\delta^{18}O$ record from Greenland (five-point smoothed) (North Greenland Ice Core Project Members, 2004); (d) sea surface temperature inferred by PCA F1, calculated from the pollen record of fore DG9603 from the mid-Okinawa Trough (D.K. Xu et al., 2013a); (e) stacked grain-size record of Chinese loess (CHILOMOS) (Yang and Ding, 2014); (g) positive index of the strength of the EAWM inferred from the AG/CS (*Aulacoseira granulata/Cyclotella stelligera*) diatom ratio (Wang et al., 2012); and sea surface temperature (SST) record from the western tropical Pacific (Stott et al., 2004; Garidel-Thoron et al., 2007).

species colonizing stabilized dunes in the deserts of NE China, *Agriophyllum squarrosum* (Chenopodiaceae) can tolerate extremely high temperatures, drought conditions and sand burial (Zhao et al., 2014). Its seeds germinate rapidly with minimal precipitation (Liu et al., 2003), and its thin roots grow very rapidly which facilitates its role as a colonizing species (Casper and Jackson, 1997; Ma et al., 2018). Moreover, even after withering, it reduces the wind velocity by at least 90% and is a source of carbon and nitrogen for infertile soils (Chen et al., 2009). Additionally, the local C_4 vegetation are sensitive to warm season precipitation (Tang et al., 1999; Huang et al., 2005), and their well-developed root system (especially in Poaceae) is critical in protecting grassland from wind erosion (Pyankov et al., 2000). Thus, C_4 vegetation, mainly Chenopodiaceae, Poaceae and Cyperaceae, were more efficient in promoting dune stabilization than other forms of localized vegetation in the deserts of NE China during the interval of ~13–5 ka. In practice, from the Last Glacial Maximum to the Holocene, the content of total organic carbon indicates that total biomass increased in the region (Fig. 7), which demonstrates that C_3 vegetation expansion was another important cause of Holocene dune stabilization.

5.3. C_4 vegetation expansion in the deserts of NE China since ~5 ka

The C_3/C_4 relative vegetation abundance increased in the study region during the mid-Holocene (Fig. 7; Huang et al., 2005), coincident with an episode of both dune mobilization (Figs. 5 and 6) and ecosystem degradation (Fig. 9; Guo et al., 2018b). Thus, the re-mobilization of dunes from ~5 ka onwards also confirms that C_4 vegetation expansion may have made a major contribution to dune stabilization.

Another distinctive characteristic of the data is a shift to an increased number of dated records of mobile and stable states at ~1.5 ka in the deserts of NE China; in addition, the number of dated records for mobile states increased at ~2.5 ka in the Mu Us and Hobq deserts, with few documented records thereafter (Fig. 5). Sun (2000) suggested that in the Mu Us desert, poor land-use practices, coupled with high wind

energy and historical droughts, led to decreased vegetation cover and dune mobilization since ~2.3 ka; this scenario is supported by the study of Yang et al. (2016) and provides a reasonable explanation for our data at ~2.5 ka. However, the number of dated records for both mobile and stable states increased at ~1.5 ka in the deserts of NE China when the climate deteriorated (Tan et al., 2003, Fig. 9f and g), which may indicate that human land-use increased the vegetation cover because of the practice of irrigation agriculture at that time. In addition, a stable isotope study of paleodiet in Inner Mongolia revealed that millet agriculture developed rapidly at ~1.5 ka and provided the staple diet for the local Tuoba Xianbei inhabitants, and for the sedentary Han Chinese farming communities who migrated to the region from the Central Plain (Zhang et al., 2015). Thus, millet agriculture at ~1.5 ka likely increased the vegetation cover in these deserts, resulting in the substantial increase in the number of dated records documenting a stable state (Figs. 5 and 7). However, climatic deterioration (Fig. 9f and g) or poor land-use practices (overgrazing and over-cultivation) after ~1.5 ka may have favored the growth of some xerophytic C_4 vegetation components (Tang et al., 1999; Wang and Ma, 2016) and induced the mobilization of unvegetated dunes (Fig. 9a). Therefore, the late Holocene C_4 vegetation expansion in the deserts of NE China (Fig. 7), likely caused by the development of millet agriculture (or overgrazing) and/or climatic deterioration, was associated with an episode of dune mobilization.

Accordingly, human activity and/or historical droughts led to a complex relationship between vegetation and dune activity in the deserts of NE China during the late Holocene. Based on our findings and previous studies, we conclude that C_4 vegetation expansion was a more important cause of late Quaternary dune stabilization than the expansion of C_3 vegetation in these deserts.

6. Conclusions

A compilation of dated records from sub-aerial sedimentary deposits during the interval of 25–0 ka in the deserts of NE China reveals episodes of dune semi-stabilization and stabilization from ~13 to 5 ka and from ~9 to 5 ka, respectively. In addition, both intervals are characterized by relatively high $\delta^{13}C_{org}$ and TOC values. However, the Otindag deserts began to stabilize at ~12 ka, later than the other deserts, leading to a northwestward trend of delayed dune stabilization in these deserts from ~13 to 9 ka. Based on the $\delta^{13}C_{org}$ values of topsoils and sections in these deserts, together with climate data, the C_3/C_4 relative vegetation abundance was strongly affected by the degree of aridity, and ultimately was responsible for promoting dune semi-stabilization with a northwestward trend, and/or stabilization throughout the entire study region.

The increased abundance of C_4 vegetation suggests that C_4 vegetation expansion in these deserts, especially of species of Chenopodiaceae, Poaceae and Cyperaceae, may have made a major contribution to dune semi-stabilization from ~13 to 9 ka, and to dune stabilization during ~9–5 ka. This conclusion is evidenced by a middle Holocene transition of dune activity and C_3/C_4 relative abundance. During the late Holocene, C_4 vegetation expansion at ~1.5 ka in the deserts of NE China, associated with a dune mobilization episode, may have resulted from the intensification of millet agriculture (or overgrazing) and/or from climatic deterioration. However, decreased vegetation cover and dune mobilization in the Mu Us and Hobq deserts occurred after ~2.5 ka, likely due to poor land-use practices and historically documented droughts. Overall, C_4 vegetation expansion was the major driving mechanism of late Quaternary dune stabilization in these deserts.

Acknowledgements

Financial support for this research was provided by the National Key R&D Program of China (Grant 2017YFA0603404), the "Strategic Priority Research Program" of the Chinese Academy of Sciences (Grants XDA19050104 and XDB26020401) and the National Natural Science Foundation of China (Grant 41272206). We thank Xu Wang and Linlin Cui for assistance in the laboratory, and Dr. Jan Bloemendal for improving an early version of the manuscript. Special thanks are extended to the editors and reviewers, who expended considerable time and effort in providing valuable suggestions and critical comments on this paper.

Appendix A. Supplementary data

Supplementary data to this article can be found online at https://doi.org/10.1016/j.quaint.2018.10.026.

References

Aitken, M.J., 1998. An Introduction to Optical Dating. Oxford University Press, Oxford, New York, Tokyo, pp. 39–46.
Bateman, M.D., Murton, J.B., 2006. The chronostratigraphy of Late Pleistocene glacial and periglacial aeolian activity in the Tuktoyaktuk Coastlands, NWT, Canada. Quat. Sci. Rev. 25, 2552–2568.
Carlson, D.H., Plummer, C.C., Carlson, L., 2015. Physical Geology, fifteenth ed. McGraw-Hill Education, New York, pp. 318–339.
Casper, B.B., Jackson, R.B., 1997. Plant competition underground. Annu. Rev. Ecol. Systemat. 28, 545–570.
Chen, B.M., Wang, G.X., Peng, S.L., 2009. Role of desert annuals in nutrient flow in arid area of Northwestern China: a nutrient reservoir and provider. Plant Ecol. 201, 401–409.
Chen, W.N., Gao, S.Y., Shao, Y.J., Zhang, H.L., 1993. Holocene pollen assemblage and climatic change in the Mu Us Sand Sea. J. Chin. Hist. Geogr. 1, 39–54 (In Chinese).
Chen, W.N., Song, J.X., Gao, S.Y.T., 1994. The characteristics of heavy mineral, organic matter, total nitrogen and phosphorus contents in Holocene deposits and their climatic significance in Mu Us Sand Sea. J. Desert Res. 14, 1–9 (In Chinese with English abstract).
Chen, Y.Y., Lu, H.Y., Zhang, E.L., Zhang, H.Y., Xu, Z.W., Yi, S.W., Wu, S.Y., 2015. Test stable carbon isotopic composition of soil organic matters as a proxy indicator of past precipitation: Study of the sand fields in northern China. Quat. Int. 372, 79–86.
Dallimore, S.R., Wolfe, S.A., Matthews Jr., J.V., Vincent, J.S., 1997. Mid-wisconsinan eolian deposits of the Kittigazuit Formation, Tuktoyaktuk Coastlands, Northwest Territories, Canada. Can. J. Earth Sci. 34, 1421–1441.
Damsté, J.S.S., Verschuren, D., Ossebaar, J., Blokker, J., Houten, R.V., Meer, M.T.J.V.D., Plessen, B., Schouten, S., 2011. A 25,000-year record of climate-induced changes in lowland vegetation of eastern equatorial Africa revealed by the stable carbon-isotopic composition of fossil plant leaf waxes. Earth Planet Sci. Lett. 302, 236–246.
Dong, G.R., Chen, H.Z., Wang, G.Y., Li, X.Z., Shao, Y.J., Jin, J., 1997. The evolution of deserts with climatic changes in China since 150 ka B.P. Sci. China, Series. D 40, 370–382.
Dong, G.R., Jin, J., Li, B.S., Gao, S.Y., Shao, Y.J., 1994. Several problems on the desertification of Horqin sandy land, Northeast China – A case study on its south area. J. Desert Res. 14, 1–9 (In Chinese with English abstract).
Dong, Y.X., Liu, Y.H., 1993. Study on the sandy desertification process of Hunshandake sandy land in recent 5000 years. Arid. Land Geogr. 16, 45–51 (In Chinese with English abstract).
Fan, A.C., Jin, Z.Y., Liu, Y.Y., Li, S.H., ZhangSun, Y.Z., Wu, Y.J., 2015. OSL chronology of traditional zinc smelting activity in Yunnan province, southwest China. Quat. Geochronol. 30, 369–373.
Gao, S.Y., Chen, W.N., Jin, H.L., Dong, G.R., Li, B.S., Yang, G.S., Liu, L.S., Guang, Y.Z., Sun, Z., Jin, J., Cao, J.X., Zhang, C.Y., 1993. Preliminary study on Holocene sand desert evolution in the northwestern fringe of China's monsoon region. Sci. China, Ser. B 23, 202–208 (In Chinese).
Gao, S.Y., Wang, G.Y., Ha, S., Su, Z.Z., 2001. A case study on desert evolution in the northwestern fringe of monsoon area, China since the last glacial epoch. Quat. Sci. 21, 66–71 (In Chinese with English abstract).
Garidel-Thoron, T.D., Rosenthal, Y., Beaufort, L., Bard, E., Sonzogni, C., Mix, A.C., 2007. A multiproxy assessment of the western equatorial Pacific hydrography during the last 30 kyr. Paleoceanogr. Paleoclimatol. 22, PA3204. https://doi.org/10.1029/2006PA001269.
Gong, Z.J., Li, S.H., Sun, J.M., Xue, L., 2013. Environmental changes in Hunshandake (Otindag) sandy land revealed by optical dating and multi-proxy study of dune sands. J. Asian Earth Sci. 76, 30–36.
Guan, C., Hasi, E., Zhang, P., Tao, B.B., Liu, D., Zhou, Y.G., 2017. Parabolic dune development modes according to shape at the southern fringes of the Hobq Desert, Inner Mongolia, China. Geomorphology 295, 654–655.
Guérin, G., Mercier, N., Adamiec, G., 2011. Dose rate conversion factors: update. Ancient TL 29, 5–8.
Guo, L.C., Wu, J.B., Xiong, S.F., Yang, S.L., 2016. New sedimentary particles sorting process based on Hydrostatic Sedimentation Method. J. Earth Sci. Environ. 38, 694–699 (In Chinese with English abstract).
Guo, L.C., Xiong, S.F., Ding, Z.L., Jin, G.Y., Wu, J.B., Ye, W., 2018b. Role of the mid-Holocene environmental transition in the decline of late Neolithic cultures in the deserts of NE China. Quat. Sci. Rev. 190, 98–113.

Guo, L.C., Xiong, S.F., Yang, P., Ye, W., Jin, G.Y., Wu, W.W., Zhao, H., 2018a. Holocene environmental changes in the Horqin desert revealed by OSL dating and $\delta^{13}C$ analyses of paleosols. Quat. Int. 469, 11–19.
Han, M.L., 2015. The Chinese Historical Geography with Fifteen Chapters. Peking University Press, Beijing (In Chinese).
Han, P., Sun, J.M., 2004. Study on OSL dating in Otindag desert. Quat. Sci. 24, 480 (In Chinese with Enghlish abstract).
He, Z., Zhou, J., Lai, Z.P., Yang, L.H., Liang, J.M., Long, H., Ou, X.J., 2010. Quartz OSL dating of sand dunes of Late Pleistocene in the Mu Us desert in northern China. Quat. Geochronol. 5, 102–106.
Huang, F., Lias, K., Xiong, S.F., Huang, F.B., 2005. Holocene grassland vegetation, climate and human impact in central eastern Inner Mongolia. Sci. China Earth Sci. 48, 1025–1039.
Huang, Y.S., Street-Perrott, F.A., Metcalfe, S.E., Brenner, M., Moreland, M., Freeman, K.H., 2001. Climate change as the dominant control on glacial-interglacial variation in C_3 and C_4 plant abundance. Science 293, 1647–1651.
Inner Mongolia-Ningxia Integrated Survey Team, Chinese Academy of Sciences, 1985. Vegetation of Inner Mongolia. Science Press, Beijing.
Jia, F.F., Lu, R.J., Gao, S.Y., Li, J.F., Liu, X.K., 2015. Holocene aeolian activities in the southeastern Mu Us Desert, China. Aeolian Res 19, 267–274.
Jiang, W.Y., Guo, Z.T., Sun, X.J., Wu, H.B., Chu, G.Q., Yuan, B.Y., Hatté, C., Guiot, J., 2006. Reconstruction of climate and vegetation changes of Lake Bayanchagan (Inner Mongolia): Holocene variability of the East Asian monsoon. Quat. Res. 65, 411–420.
Jin, H.L., Su, Z.Z., Sun, L.Y., Su, Z., Zhang, H., Hong, Z., Jin, L.Y., 2004. Holocene climatic change in Hunshandake Desert. Chin. Sci. Bull. 49, 1730–1735.
Jin, H.L., Su, Z.Z., Sun, Z., 2003. Characters of chemical elements in strata of middle and late Holocene in Hunshandake Desert and the indicating climatic changes. J. Desert Res. 23, 366–371 (In Chinese with English abstract).
Jin, H.L., Sun, L.Y., Sun, Z., 2010. Millennial-scale evolution of Hunshandake Desert and climate change during the Holocene in Inner Mongolia, northern China. Sci. in Cold and Arid Reg. 2, 0505–0513.
Kang, S.K., Wang, X.L., Lu, Y.C., Liu, W.G., Song, Y.G., Wang, N., 2015. A high-resolution quartz OSL chronology of the Talede loess over the past ~30ka and its implications for dust accumulation in the Ili Basin, Central Asia. Quat. Geochronol. 30, 181–187.
Leighton, C.L., Bailey, R.M., Thomas, D.S.G., 2014. Interpreting and modelling late Quaternary dune accumulation in the southern Arabian Peninsula. Quat. Sci. Rev. 102, 1–13.
Li, H.W., Yang, X.P., 2016. Spatial and temporal patterns of aeolian activities in the desert belt of northern China revealed by dune chronologies. Quat. Int. 410, 58–68.
Li, S., Sun, W., Li, X.Z., Zhang, B., 1995. Sedimentary characteristics and environmental evolution of Otindag Sandy Land in Holocene. J. Desert Res. 15, 323–331 (In Chinese with English abstract).
Li, S.H., Chen, Y.Y., Li, B., Sun, J.M., Yang, L.R., 2007. OSL dating of sediments from deserts in northern China. Quat. Geochronol. 2, 23–28.
Li, S.H., Sun, J.M., 2006. Optical dating of Holocene dune sands from the Hulun Buir Desert, northeastern China. Holocene 16, 457–462.
Li, S.H., Sun, J.M., Li, B., 2012. Holocene environmental changes in central Inner Mongolia revealed by luminescence dating of sediments from the Sala Us River valley. Holocene 22, 397–404.
Li, S.H., Sun, J.M., Zhao, H., 2002. Optical dating of dune sands in the northeastern deserts of China. Palaeogeogr. Palaeoclimatol. Palaeoecol. 181, 419–429.
Li, Y.Y., Lu, J.F., 1996. The sporo-pollen records and vegetation and climate history in Songnen Sandy Land since Epipleistocene. J. Desert Res. 16, 338–344 (In Chinese with English abstract).
Liu, B., Jin, H.L., Sun, L.Y., Sun, Z., Niu, Q.H., Xie, S.B., Li, G.H., 2014. Holocene moisture change revealed by the Rb/Sr ratio of aeolian deposits in the southeastern Mu Us Desert, China. Aeolian Res 13, 109–119.
Liu, B., Jin, H.L., Sun, L.Y., Sun, Z., Zhao, S., 2015a. Geochemical evidence for Holocene millennial-scale climatic and environmental changes in the south-eastern Mu Us Desert, northern China. Int. J. Earth Sci. 104, 1889–1900.
Liu, J., Wang, Y., Yao, P.Y., Chi, Z.Q., Li, T.D., Geng, S.F., 2015b. A study of paleoclimate changes in east Inner Monglia since the Last deglaciation on the basis of aeolian sand-paleosoil series geochemical records. Chin. Geol. 42, 1103–1114 (In Chinese with English abstract).
Liu, B., Jin, H.L., Sun, Z., 2011. Climate change in east Horqin Sandy Land since 6.0 ka BP. J. Desert Res. 31, 1398–1405 (In Chinese with English abstract).
Liu, B., Jin, H.L., Sun, Z., 2013. Desert evolutin and climate change in the Horqin Sandy Land in middle and late Holocene. J. Desert Res. 33, 77–86 (In Chinese with English abstract).
Liu, K., Lai, Z.P., 2012. Chronology of Holocene sediments from the archaeological Salawusu site in the Mu Us Desert in China and its palaeoenvironmental implications. J. Asian Earth Sci. 45, 247–255.
Liu, L., Chen, X.C., 2012. The Archaeology of China: From the Late Paleolithic to the Early Bronze Age. Cambridge University Press, Cambridge, U.K.
Liu, L., Qiao, Y.S., Hao, Z.G., 2016a. Black carbon concentration and isotopic composition of surface sand from deserts and dune fields in Northern China. Palaeogeogr. Palaeoclimatol. Palaeoecol. 445, 1–7.
Liu, M., Hasi, E., Sun, Y., 2016b. Variation in grain size and morphology of an inland parabolic dune during the incipient phase of stabilization in the Hobq Desert, China. Sediment. Geol. 337, 100–112.
Liu, M.G., 2010. Atlas of Physical Geography of China, third ed. China Map Press, Beijing, pp. 41 (In Chinese).
Liu, M.Z., Jiang, G.M., Niu, S.L., Li, Y.G., Gao, L.M., Ding, L., Peng, Y., 2003. Photosynthetic response to soil water contents of an annual pioneer C_4, grass (*Agriophyllum squarrosum*) in Hunshandak Sandland, China. Photosynthetica 41, 293–296.
Liu, X., Hou, L.Y., 1995. Study on the relationship between the developed characteristics of Holocene epoch strata and climatic fluctation in the east Inner Monglia. Geol. Inn. Mong. Z1, 54–62 (In Chinese with English abstract).
Lu, H.Y., Mason, J.A., Stevens, T., Zhou, Y.L., Yi, S.W., Miao, X.D., 2011. Response of surface processes to climatic change in the dunefields and Loess Plateau of North China during the late Quaternary. Earth Surf. Process. Landforms 36, 1590–1603.
Lu, H.Y., Miao, X.D., Zhou, Y.L., Mason, J.A., Swinehart, J.B., Zhang, J.F., Zhou, L.P., Yi, S.W., 2005. Late Quaternary aeolian activity in the Mu Us and Otindag dune fields (north China) and lagged response to insolation forcing. Geophys. Res. Lett. 32, L2176. https://doi.org/10.1029/2005GL024560.
Lu, H.Y., Yi, S.W., Liu, Z.Y., Mason, J.A., Jiang, D.B., Cheng, J., Stevens, T., Xu, Z.W., Zhang, E.L., Jin, L.Y., Zhang, Z.H., Guo, Z.T., Wang, Y., Otto-Bliesner, B., 2013. Variation of East Asian Monsoon precipitation during the past 21 k.y. and potential CO_2 forcing. Geology 41, 1023–1026.
Lu, H.Y., Zhou, Y.L., Liu, W.G., Mason, J., 2012. Organic stable carbon isotopic composition reveals late Quaternary vegetation changes in the dune fields of northern China. Quat. Res. 77, 433–444.
Lu, R.J., Wang, Y.J., Zhang, D.S., 2010. Climate changes and desert evolution of Mu Us Desert since 15 ka BP. J. Desert Res. 30, 273–277 (In Chinese with English abstract).
Lubke, R.A., Hertling, U.M., 2001. The role of European marram grass in dune stabilization and succession near Cape Agulhas, South Africa. J. Coast Conserv. 7, 171–182.
Ma, J., 2012. OSL Dating of Holocene Sequence and Palaeoclimate Change Record in Southeastern Margin of Mu Us Desert, North China. Master's Thesis,. Northwest University, Xi'an.
Ma, J., Yue, L.P., Yang, L.H., Sun, L., Xu, Y., 2011. OSL dating of Holocene sequence and palaeoclimate change record in southeastern margin of Mu Us desert, North China. Quat. Sci. 31, 120–129 (In Chinese with English abstract).
Ma, Z.Q., Guo, D.S., Xu, X.L., Lu, M.Z., Bardgett, R.D., Eissenstat, D.M., Mccormack, M.L., Hedin, L.O., 2018. Evolutionary history resolves global organization of root functional traits. Nature 555, 94–97.
Mason, J.A., Lu, H.Y., Zhou, Y.L., Miao, X., Swinehart, J.B., Liu, Z.Y., Goble, R.J., Yi, S.W., 2009. Dune mobility and aridity at the desert margin of northern China at a time of peak monsoon strength. Geology 37, 947–950.
Munyikwa, K., 2005. Synchrony of Southern Hemisphere Late Pleistocene arid episodes: A review of luminescence chronologies from arid aeolian landscapes south of the Equator. Quat. Sci. Rev. 24, 2555–2583.
Munyikwa, K., Rittenour, T.M., Feathers, J.K., 2017. Temporal constraints for the Late Wisconsinan deglaciation of western Canada using eolian dune luminescence chronologies from Alberta. Palaeogeogr. Palaeoclimatol. Palaeoecol. 470, 147–165.
Niu, D.F., Li, B.S., Wang, F.N., Cheng, Q., Shu, P.X., Wen, X.H., Chen, M., 2015. Holocene climate fluctuations from the record of trace elements in the Mu Us Desert: evidence from the DGS1 segment of the Salawusu River Valley. Acta Sedimentol. Sin. 33, 735–743 (In Chinese with English abstract).
North Greenland Ice Core Project members, 2004. High-resolution record of Northern Hemisphere climate extending into the last interglacial period. Nature 431, 147–151.
Prescott, J.R., Hutton, J.T., 1994. Cosmic-ray contributions to dose-rates for luminescence and ESR dating: large depths and long-term time variations. Radiat. Meas. 23, 497–500.
Pyankov, V.I., Gunin, P.D., Tsoog, S., Black, C.C., 2000. C_4 plants in the vegetation of Mongolia: their natural occurrence and geographical distribution in relation to climate. Oecologia 123, 15–31.
Pye, K., Tsoar, H., 2009. Aeolian Sand and Sand Dunes. Springer, Berlin Heidelberg.
Qiu, S.W., Li, Q.S., Xia, Y.M., 1992. Paleosols of sandy lands and environmental changes in the western plain of Northeast China during Holocene. Quat. Sci. 3, 224–232 (In Chinese with English abstract).
Rao, Z.G., Guo, W.K., Cao, J.T., Shi, F.X., Jiang, H., Li, C.Z., 2017. Relationship between the stable carbon isotopic composition of modern plants and surface soils and climate: A global review. Earth Sci. Rev. 165, 110–119.
Rao, Z.G., Jia, G.D., Zhu, Z.Y., Wu, Y., Zhang, J.W., 2008. Comparison of the carbon isotope composition of total organic carbon and long-chain *n*-alkanes from surface soils in eastern China and their significance. Chin. Sci. Bull. 53, 3921–3927.
Reimer, P.J., Bard, E., Bayliss, A., Beck, J.W., Blackwell, P.G., Bronk Ramsey, C., Buck, C.E., Cheng, H., Edwards, R.L., Friedrich, M., Grootes, P.M., Guilderson, T.P., Haflidason, H., Hajdas, I., Hatte, C., Heaton, T.J., Hoffmann, D.L., Hogg, A.G., Hughen, K.A., Kaiser, K.F., Kromer, B., Manning, S.W., Niu, M., Reimer, R.W., Richards, D.A., Scott, E.M., Southon, J.R., Staff, R.A., Turney, C.S.M., van der Plicht, J., 2013. IntCal13 and Marine13 radiocarbon age calibration curves, 0–50,000 years cal BP. Radiocarbon 55, 1869–1877.
Reitz, M.D., Jerolmack, D.J., Ewing, R.C., Martin, R.L., 2010. Barchan-parabolic dune pattern transition from vegetation stability threshold. Geophys. Res. Lett. 37, L19402. https://doi.org/10.1029/2010GL044957.
Ren, M.E., Yang, R.Z., Bao, H.S., 1985. An Outline of China's Physical Geography. Foreign Languages Press, Beijing, pp. 346–361.
Roskin, J., Porat, N., Tsoar, H., Dan, G.B., Zander, A.M., 2011. Age, origin and climatic controls on vegetated linear dunes in the northwestern Negev Desert (Israel). Quat. Sci. Rev. 30, 1649–1674.
Stott, L., Cannariato, K., Thunell, R., Haug, G.H., Koutavas, A., Lund, S., 2004. Decline of surface temperature and salinity in the western tropical Pacific Ocean in the Holocene epoch. Nature 431, 56–59.
Stuiver, M., Reimer, P.J., 1993. Extended ^{14}C data base and revised CALIB 3.0 ^{14}C age calibration program. Radiocarbon 35, 215–230.
Sun, J.M., 2000. Origin of aeolian sand mobilization during the past 2300 years in the Mu Us Desert, China. Quat. Res. 53, 78–88.
Sun, J.M., Ding, Z.L., Liu, T.S., Rokosh, D., Rutter, N., 1999. 580,000-year environmental reconstruction from aeolian deposits at the Mu Us Desert margin, China. Quat. Sci. Rev. 18, 1351–1364.

Sun, J.M., Li, S.H., Han, P., Chen, Y.Y., 2006. Holocene environmental changes in the central Inner Mongolia, based on single-aliquot-quartz optical dating and multi-proxy study of dune sands. Palaeogeogr. Palaeoclimatol. Palaeoecol. 233, 51–62.
Sun, J.M., Muhs, D.R., 2007. Dunefields: mid-latitudes. In: Elias, S.A. (Ed.), The Encyclopedia of Quaternary Sciences. Elsevier, Amsterdam, pp. 607–626.
Tan, M., Liu, T.S., Hou, J.S., Qin, X.G., Zhang, H.C., Li, T.Y., 2003. Cyclic rapid warming on centennial-scale revealed by a 2650-year stalagmite record of warm season temperature. Geophys. Res. Lett. 30, 1617. https://doi.org/10.1029/2003GL017352.
Tang, H.P., Liu, S.R., Zhang, X.S., 1999. The C_4 plants in Inner Mongolia and their eco-geographical characteristics. Acta Bot. Sin. 41, 420–424 (In Chinese with English abstract).
Tsoar, H., 2005. Sand dunes mobility and stability in relation to climate. Physica A 357, 50–56.
Tsoar, H., Pye, K., 1987. Dust transport and the question of desert loess formation. Sedimentology 34, 139–153.
UNEP (United Nations Environment Programme), 1997. World Atlas of Desertification 2ED. UNEP, London.
Wang, G.A., Li, J.Z., Liu, X.Z., Li, X.J., 2013. Variations in carbon isotope ratios of plants across a temperature gradient along the 400 mm isoline of mean annual precipitation in north China and their relevance to paleovegetation reconstruction. Quat. Sci. Rev. 63, 83–90.
Wang, L., Li, J.J., Lu, H.Y., Gu, Z.Y., Rioual, P., Hao, Q.Z., Mackay, A.M., Jiang, W.Y., Cai, B.G., Xu, B., Han, J.T., Chu, G.Q., 2012. The East Asian winter monsoon over the last 15,000 years: its links to high-latitudes and tropical climate systems and complex correlation to the summer monsoon. Quat. Sci. Rev. 32, 131–142.
Wang, P.F., 1992. Priliminary study on the environmental changes of Hulun Buir Sandy land since the Holocene. J. Desert Res. 12, 13–19 (In Chinese with English abstract).
Wang, R.Z., 2002. Photosynthetic pathways and life forms in different grassland types from North China. Photosynthetica 40, 243–250.
Wang, R.Z., 2007. C_4 plants in the deserts of China: occurrence of C_4 photosynthesis and their morphological functional types. Photosynthetica 45, 167–171.
Wang, R.Z., Ma, L.N., 2016. Climate-driven C_4 plant distributions in China: divergence in C_4 taxa. Sci. Rep. 6 (27977). https://doi.org/10.1038/srep27977.
Wang, X.Q., Jiang, J., Lei, J.Q., Zhang, W.M., Qian, Y.B., 2003. Distribution of ephemeral plants and their significance in dune stabilization in Gurbantunggut Desert. J. Geogr. Sci. 13, 323–330.
Wen, R.L., Xiao, J.L., Chang, Z.G., Zhai, D.Y., Xu, Q.H., Li, Y.C., Itoh, S., Lomtatidze, Z., 2010. Holocene climate changes in the mid-high latitude monsoon margin reflected by the pollen record from Hulun Lake, northeastern Inner Mongolia. Quat. Res. 73, 293–303.
Wen, R.L., Xiao, J.L., Fan, J.W., Zhang, S.R., Yamagata, H., 2017. Pollen evidence for a mid-Holocene East Asian summer monsoon maximum in northern China. Quat. Sci. Rev. 176, 29–35.
Wintle, A.G., Murray, A.S., 2006. A review of quartz optically stimulated luminescence characteristics and their relevance in single-aliquot regeneration dating protocols. Radiat. Meas. 41, 369–391.
Wolfe, S.A., Huntley, D.J., Ollerhead, J., 2004. Relict late Wisconsinan dune fields of the northern Great Plains, Canada. Géogr. Phys. Quaternaire 58, 323–336.
Xiao, J.L., Xu, Q.H., Nakamura, T., Yang, X.L., Liang, W.D., Inouchi, Y., 2004. Holocene vegetation variation in the Daihai Lake region of north-central China: a direct indication of the Asian monsoon climatic history. Quat. Sci. Rev. 23, 1669–1679.
Xu, D.K., Lu, H.Y., Wu, N.Q., Liu, Z.X., Li, T.G., Shen, C.M., Wang, L., 2013a. Asynchronous marine-terrestrial signals of the last deglacial warming in East Asia associated with low- and high-latitude climate changes. Proc. Natl. Acad. Sci. U. S. A 110, 9657–9662.
Xu, Z.W., Lu, H.Y., Yi, S.W., Zhou, Y.L., Mason, J.A., Wang, X.Y., Chen, Y.Y., Zhu, F.Y., Zhang, H., Zhai, X.M., 2013b. Spatial variations of the Mu Us dune field (north central China) during the Last Glacial Maximum and Holocene Optimum. Quat. Sci. 33, 218–227 (In Chinese with English abstract).
Xu, Q.H., Kong, Z.C., Chen, X.D., Yang, X.L., Liang, W.D., Sun, L.M., 2002b. Discussion on the environment changes and the effects of human impacts in the east Ordos Plateau since 4 000aB.P. Quat. Sci. 22, 105–112 (In Chinese with English abstract).
Xu, Q.H., Yang, Z.J., Cui, Z.J., Yang, X.L., Liang, W.D., 2002a. A study on pollen analysis of Qiguoshan Section and ancestor living environment in Chifeng Area, Nei Mongol. Sci. Geogr. Sin. 22, 453–457 (In Chinese with English abstract).
Xu, Z., Mason, J.A., Lu, H., 2015b. Vegetated dune morphodynamics during recent stabilization of the Mu Us dune field, north-central China. Geomorphology 228, 486–503.
Xu, Z.W., Lu, H.Y., Yi, S.W., Vandenberghe, J., Mason, J.A., Zhou, Y.L., Wang, X.Y., 2015a. Climate-driven changes to dune activity during the Last Glacial Maximum and deglaciation in the Mu Us dune field, north-central China. Earth Planet Sci. Lett. 427, 149–159.
Yan, N., Baas, A.C.W., 2015. Parabolic dunes and their transformations under environmental and climatic changes: Towards a conceptual framework for understanding and prediction. Global Planet. Change 124, 123–148.
Yan, N., Baas, A.C.W., 2017. Environmental controls, morphodynamic processes, and ecogeomorphic interactions of barchan to parabolic dune transformations. Geomorphology 278, 209–237.
Yang, L.H., Wang, T., Zhou, J., Lai, Z.P., Long, H., 2012a. OSL chronology and possible forcing mechanisms of dune evolution in the Horqin dunefield in northern China since the Last Glacial Maximum. Quat. Res. 78, 185–196.
Yang, X.P., Li, H.W., Conacher, A., 2012b. Large-scale controls on the development of sand seas in northern China. Quat. Int. 250, 74–83.
Yang, L.H., Wang, T., Long, H., He, Z., 2017. Late Holocene dune mobilization in the Horqin dunefield of northern China. J. Asian Earth Sci. 138, 136–147.
Yang, L.R., Ding, Z.L., 2013. Expansion and contraction of Hulun Buir Dunefield in northeastern China in the last late glacial and Holocene as revealed by OSL dating. Environ. Earth Sci. 68, 1305–1312.
Yang, L.R., Yue, L.P., 2011. The environmental transformation from late last glacial to Holocene of Otindag sandyland. J. Earth Environ. 2, 301–306 (In Chinese with English abstract).
Yang, L.R., Yue, L.P., 2013. Horqin dunefield in northeastern China in the last late glacial and Holocene as revealed by OSL dating. Quat. Sci. 33, 260–268 (In Chinese with English abstract).
Yang, S.L., Ding, Z.L., 2014. A 249 kyr stack of eight loess grain size records from northern China documenting millennial-scale climate variability. Geochem. Geophys. Geosyst. 15, 798–814.
Yang, S.L., Ding, Z.L., Li, Y.Y., Wang, X., Jiang, W.Y., Huang, X.F., 2015a. Warming-induced northwestward migration of the East Asian monsoon rain belt from the Last Glacial Maximum to the mid-Holocene. Proc. Natl. Acad. Sci. U. S. A 112, 13178–13183.
Yang, X.P., Scuderi, L.A., Wang, X.L., Scuderi, L.J., Zhang, D.G., Li, H.W., Forman, S., Xu, Q.H., Wang, R.C., Huang, W.W., Yang, S.X., 2015b. Groundwater sapping as the cause of irreversible desertification of Hunshandake Sandy Lands, Inner Mongolia, northern China. Proc. Natl. Acad. Sci. U. S. A 112, 702–706.
Yang, X.P., Forman, S., Hu, F.G., Zhang, D.G., Liu, Z.T., Li, H.W., 2016. Initial insights into the age and origin of the Kubuqi sand sea of northern China. Geomorphology 259, 30–39.
Yang, X.P., Wang, X.L., Liu, Z.T., Li, H.W., Ren, X.Z., Zhang, D.G., Ma, Z.B., Rioual, P., Jin, X.D., Scuderi, L., 2013. Initiation and variation of the dune fields in semi-arid northern China – with a special reference to the Hunshandake Sandy Land, Inner Mongolia. Quat. Sci. Rev. 78, 369–380.
Yang, X.P., Zhu, B., Wang, X., Li, C., Zhou, Z., Chen, J., Wang, X., Yin, J., Lu, Y., 2008. Late Quaternary environmental changes and organic carbon density in the Hunshandake Sandy Land, eastern Inner Mongolia, China. Global Planet. Change 61, 70–78.
Yi, S.W., Lu, H.Y., Zeng, L., Xu, Z.W., 2013. Paleoclimate changes and reconstruction of the border of Horqin dunefield (northeastern China) since the Last Glacial Maximum. Quat. Sci. 33, 206–217 (In Chinese with English abstract).
Zeng, L., Lu, H.Y., Yi, S.W., Chen, Y.Y., Zhu, F.Y., 2013. Environment changes of Hulun Buir dunefield in northeastern China during the Last Glacial Maximum and Holocene Optimum. Quat. Sci. 33, 243–251 (In Chinese with English abstract).
Zhang, G.W., Hu, Y.W., Wang, L.M., Cao, C.M., Li, X.S., Wu, X.N., Sun, Z.D., Chen, F.S., Bai, J.S., Lv, P., Song, G.D., Wang, C.S., Richards, M.P., 2015. A paleodietary and subsistence strategy investigation of the Iron Age Tuoba Xianbei site by stable isotopic analysis: A preliminary study of the role of agriculture played in pastoral nomad societies in northern China. J. Archaeol. Sci. Rep. 2, 699–707.
Zhang, S.R., Xiao, J.L., Xu, Q.H., Wen, R.L., Fan, J.W., Huang, Y., Yamagata, H., 2018. Differential response of vegetation in Hulun Lake region at the northern margin of Asian summer monsoon to extreme cold events of the last deglaciation. Quat. Sci. Rev. 190, 57–65.
Zhang, X.Y., Zhou, Y.L., Pang, J.L., Lu, H.Y., Huang, C.C., Zhou, L., Gu, H.L., 2012. The relationship between environmental changes and human actives during the Medieval Warm Period and the Little Ice Age in Otindag sandland bu OSL dating. Quat. Sci. 32, 535–546 (In Chinese with English abstract).
Zhao, H., Lu, Y.C., Yin, J.H., 2007. Optical dating of Holocene sand dune activities in the Horqin sand-fields in Inner Mongolia, China, using the SAR protocol. Quat. Geochronol. 2, 29–33.
Zhao, P., Capella-Gutiérrez, S., Shi, Y., Zhao, X., Chen, G.X., Gabaldón, T., Ma, X.F., 2014. Transcriptomic analysis of a psammophyte food crop, sand rice (*Agriophyllum squarrosum*) and identification of candidate genes essential for sand dune adaptation. BMC Genomics 15, 872. https://doi.org/10.1186/1471-2164-15-872.
Zhao, S., Xia, D.S., Jin, H.L., Wen, Y.L., Liu, J.B., Liu, B., Li, G.H., 2013. High-resolution climate evolution record of the Horqin sandy land since about 5000cal. aB.P. Quat. Sci. 33, 283–292 (In Chinese with English abstract).
Zhou, W.J., An, Z.S., Jull, A.J.T., Donahue, D.J., Head, M.J., 1998. Reappraisal of Chinese Loess Plateau stratigraphic sequences over the last 30,000 years: precursors of an important Holocene monsoon climatic event. Radiocarbon 40, 905–913.
Zhou, W.J., Dodson, J., Head, M.J., Li, B.S., Hou, Y.J., Lu, X.F., Donahue, D.J., Jull, A.J.T., 2002. Environmental variability within the Chinese desert-loess transition zone over the last 20000 years. Holocene 12, 107–112.
Zhou, W.J., Head, M.J., Deng, L., 2001. Climate changes in northern China since the late Pleistocene and its response to global change. Quat. Int. 83–85, 285–292.
Zhou, W.J., Head, M.J., Lu, X.F., An, Z.S., Jull, A.J.T., Donahue, D., 1999. Teleconnection of climatic events between East Asia and polar, high latitude areas during the last deglaciation. Palaeogeogr. Palaeoclimatol. Palaeoecol. 152, 163–172.
Zhou, Y.L., Lu, H.Y., Mason, J.A., Miao, X.D., Swinehart, J.B., Goble, R.J., 2008. Optically stimulated luminescence dating of aaeolian sand in the Otindag dunefield and Holocene climate change. Sci. China Earth Sci. 51, 837–847.
Zhou, Y.L., Lu, H.Y., Zhang, J.F., Mason, J.A., Zhou, L.P., 2009. Luminescence dating of sand-loess sequences and response of Mu Us and Otindag sand fields (north China) to climatic changes. J. Quat. Sci. 24, 336–344.
Zhou, Y.L., Lu, H.Y., Zhang, J.F., Zhou, L.P., Miao, X.D., Mason, J.A., 2005. Active and inactive phases of sand dune in Mu Us and Otindag sandlands during late Quaternary suggested by OSL dating. J. Desert Res. 25, 342–350 (In Chinese with English abstract).
Zhou, Y.L., Lu, H.Y., Zhang, X.Y., Yi, S.W., 2013. Changes of the border of Otindag sand field (northern China) during the Last Glacial Maximum and Holocene Optimum. Quat. Sci. 33, 228–242 (In Chinese with English abstract).
Zhu, Z., Wu, Z., Liu, S., Di, X., 1980. An Outline of Chinese Deserts. Science Press, Beijing (in Chinese).